Final Technical Report

to the National Aeronautics and Space Administration

APPLICATION OF LASER RANGING
AND VLBI DATA TO A STUDY
OF PLATE TECTONIC DRIVING FORCES

Principal Investigator: Sean C. Solomon

Associate Professor of Geophysics

SS # ███████

617-253-3786

NASA Cooperative Agreement NCC 5-14

1 May 1979 to 30 April 1980

Massachusetts Institute of Technology

77 Massachusetts Avenue

Cambridge, MA 02139

N80-26979

This is the Final Technical Report for the NASA Cooperative Agreement NCC 5-14 "Application of Laser Ranging and VLBI Data to a Study of Plate Tectonic Driving Forces" for the funding period 1 May 1979 through 30 April 1980. The broad goals of our research under this Cooperative Agreement have been to investigate the conditions under which changes in plate driving or resistive forces associated with plate boundary earthquakes will be measurable with laser ranging or VLBI and to pinpoint those aspects of plate forces that can be characterized by such measurements.

This Report is divided into three parts, each describing a specific research task completed during the past year and contributing to the broad goals of the project: (1) analytic solutions for two-dimensional stress diffusion in a viscoelastic plate following earthquake faulting on a finite fault; (2) finite-element solutions for three-dimensional stress diffusion in a viscoelastic Earth following earthquake faulting; and (3) quantitative constraints from modeling of global intraplate stress on the magnitude of deviatoric stress in the lithosphere

1. Introduction

Most of the earthquakes today occur along plate boundaries. Strain energy accumulates and releases at these boundaries ,deforms surfaces, and causes dammage. The understanding of earthquake mechanisms is becoming more important in order to forecast and, further, to predict earthquakes.

The migration of large earthquakes was first studied by Mogi (1968a,1968b). Delsemme and Smith (1979) have quantitatively analyzed the migration pattern along many plate boundaries around the world; periodic trends in space and time are obtained. A qualitative mechanism concerning a possibly deep-seated migration front of stress triggering earthquakes along its propagating direction (Scholz, 1977) is the general explanation to the migration phenomena. However, the relationship between large earthquakes at greater time-distance intervals is less clear. Recently, the migration of crustal deformation has been discovered in many tectonic areas (Kasahara,1979). Dispersion and dissipation of the deformation waveform are also noted as characteristics. Extrapolating the migration path back toward the ocean, the deformation front seems to have originated from the vicinity of the trench. It is supposed that either a repeated irregular aseismic plate motion generates the deformation events, or that it

results from a periodic seismic slip at a plate boundary. Quantitative study has been carried out by Yang (1979). Analytical solution about the stress (or displacement) response in time and space due to earthquake disturbances at the plate boundary is still necessary to obtain physical insights of the migration process.

In previous reports, we have studied the effect of earthquakes on plate motion using analytical one-dimensional viscoelastic and two-dimensional elastic models. The models incorporated the interactions between the elastic lithosphere and the asthenosphere. With periodic earthquakes the one dimensional study show significant fluctuations of displacement field at large distances from the plate boundary. The two dimensional model consists of two finite elastic rectangular plates , one overlying the other, with different thicknesses as shown in figure 1. Applying a unit displacement at the plate boundary suggests that the instantaneous elastic deformations are significant within a distance equivalent to the length of the fault rupture.

In this report, we extend our two dimensional elastic study to a viscoelastic model using the correspondence principle (Christiansen, 1971). A Maxwellian viscoelastic asthenosphere is assumed and time-dependent deformations in the lithosphere are calculated.

2. Two Dimensional Time-Dependent Solution of Stress Propagation

Time dependent solutions of horizontal stress and strain propagation in lithosphere can be obtained using correspondence principle (Christiansen, 1971). Figure 1 shows a finite two dimensional plate with length L, width 2C, thickness H1 overlying a second layer of the same size and thickness H2. We choose a simple Maxwellian viscoelastic behavior in shear for the asthenosphere, and an elastic response in the lithosphere. The hatched area represents the finite rupture zone at the plate boundary with total width 2D. The x-coordinate is normal to the plate boundary and the y-coordinate is parallel to the plate boundary. The origin is located at the center of the "fault". We are calculating the stress and displacement at specific distances from the origin in both x and y directions.

Starting with the equations of motion in the two dimensional elastic case :

$$2 \ \partial^2 u / \partial x^2 + (1-\nu) \ \partial^2 u / \partial y^2 + (1+\nu) \ \partial^2 v / (\partial x \cdot \partial y)$$
$$= 2\mu(1-\nu^2) u / (E \cdot H1 \cdot H2) \tag{1a}$$

$$2 \ \partial^2 v / \partial y^2 + (1-\nu) \ \partial^2 v / \partial x^2 + (1+\nu) \ \partial^2 u / (\partial x \cdot \partial y) \tag{1b}$$
$$= 2\mu(1-\nu^2) v / (E \cdot H1 \cdot H2)$$

where u, v are displacement field in x, y direction respectively. ν is the Poisson's ratio, E is the Young's

modulus of the lithosphere, and μ is the shear modulus of the asthenosphere.

Take Laplace transform of (1a) and (1b) and non-dimensionalize

u, v by the initial displacement at rupture zone,

x, y by H1, the thickness of the lithosphere, and

t by T, the relaxation time of the asthenosphere,

we obtain:

$$2\partial^2 U/\partial X^2 + (1-\nu)\, \partial^2 U/\partial Y^2) + (1+\nu)\, \partial^2 V/(\partial X \cdot \partial Y) \qquad (2a)$$
$$= 2\,(H1\cdot\mu)/(E\cdot H2)\,(1-\nu^2)\,T\cdot s\cdot U/(T\cdot s+1)$$

$$2\,\partial^2 V/\partial Y^2 + (1-\nu)\, \partial^2 V/\partial X^2 + (1+\nu)\, \partial^2 U/(\partial X \cdot \partial Y) \qquad (2b)$$
$$= 2\,(H1\cdot\mu)/(E\cdot H2)\,(1-\nu^2)\,T\cdot s\cdot V/(T\cdot s+1)$$

where X and Y are the non-dimensional x and y, U and V are the non-dimensional u and v in Laplace domain, T is the relaxation time of the asthenosphere, and s is the Laplace parameter.

The above two equations are similar to those in our two dimensional elastic case except that there is a time dependent factor $Ts/(Ts+1)$ at the right hand side of the equations.

We can further simplify the equations (2a) and (2b) into:

$$\nabla^2 \psi = k^2/2 \tag{3}$$

$$\nabla^2 \varphi = k^2/(1-\nu) \tag{4}$$

where ∇^2 is the laplacian operator in two dimension and

$$\psi = \partial U/\partial X + \partial V/\partial Y$$

$$\varphi = \partial U/\partial Y - \partial V/\partial X$$

$$k^2(s) = 2(\mu \cdot H1)/(E \cdot H2)(1-\nu^2) \, Ts/(Ts+1)$$

A set of solutions that satisfies equations (3) and (4) is

$$U(x,y) = \sum_{m=0}^{\infty} \cos \alpha y \cdot \left\{ \frac{a}{a^2-\alpha^2}(A_1 e^{aX} - A_2 e^{-aX}) + \frac{\alpha}{b^2-\alpha^2}(B_3 e^{bX} + B_4 e^{-bX}) \right\}$$

$$+ \sum_{m=0}^{\infty} \sin \alpha y \left\{ \frac{a}{a^2-\alpha^2}(A_3 e^{aX} - A_4 e^{-aX}) - \frac{\alpha}{b^2-\alpha^2}(B_1 e^{bX} + B_2 e^{-bX}) \right\}$$

$$V(x,y) = \sum_{m=0}^{\infty} \cos \alpha y \left\{ \frac{\alpha}{a^2-\alpha^2}(A_3 e^{ax} + A_4 e^{-ax}) + \frac{b}{b^2-\alpha^2}(B_1 e^{bx} - B_2 e^{-bx}) \right\}$$

$$+ \sum_{m=0}^{\infty} \sin \alpha y \left\{ \frac{-\alpha}{a^2-\alpha^2}(A_1 e^{ax} + A_2 e^{-ax}) - \frac{b}{b^2-\alpha^2}(B_3 e^{bx} - B_4 e^{-bx}) \right\}$$

where

$$\alpha = \frac{m\pi}{c}$$

$$a = \sqrt{\alpha^2 + \frac{k^2}{2}}$$

$$b = \sqrt{\alpha^2 + \frac{k^2}{1-\nu}}$$

The coefficients A1,A2,.....,B3,B4 are functions of m. Notice that the displacement fields decay exponentially with X and the decay constants, a and b, are time-dependent.

Boundary conditions

Great earthquakes and their aftershocks only occur along a small portion of the boundary. To simulate a finite rupture zone, we apply a unit displacement in the hatched area from y=-D to y=D throughout the thickness H1 (see figure 1). The remainder of this boundary is fixed in the x direction. Figure 2 gives a top view of the model and a brief summary of the boundary conditions. Motion in the y direction is allowed at the trench. The ridge side is assumed to be stress free. Along the other two boundaries, we confine the motion to the y direction and ignore friction.

Mathematically, these conditions are:

$$U(0,Y) = D/C + 2\sin(\alpha \cdot D)\cos(\alpha \cdot Y)/(\alpha \cdot C)$$

$$\sigma_x(L,Y) = \tau_{xy}(L,Y) = 0$$

$$V(X, \pm C) = 0$$

Using these boundary conditions and equations (3), (4), we obtain time-dependent coefficients with the same form as those in two dimensional elastic case . Inverting to the time domain from the Laplace domain with the Fast Fourier transform, simple numerical solution results (Dubner and Abate,1968).

Results

In most of the figures shown below, we use two kinds of units, dimensionless unit and dimensional unit. For dimensional unit we refer to

```
L=5000km
C=4000km
H1=100km
H2=80km
D=800km
μ=.7e11 dyne/cm
E=1.7e12 dyne/cm
T=7e7 sec
η=5e19 poise
```

We assume 1.6 meters horizontal displacement normal to the rupture zone to simulate earthquake slip.

The u displacement parallel to the x-axis at distances of 400,800,and 1200 km from the trench are shown in figure 3. At time 0, the disturbance at plate boundary effects only adjacent regions of the plate. As time increases, it gradually propagates deeper into the plate.

The velocity as a function of time along the x-axis is shown in figure 4. The effect of the asthenospheric stress relaxation is obvious. The shape of the velocity curve is similar to those in our one dimensional model, which assumes an infinite fault; however, the magnitude of the maximum velocity is smaller than the one dimensional case. For example, the maximum velocity at 400 km from the fault is about 25% small. This suggests that fault length is one important factor for propagation velocity.

Figure 5 shows the v displacement along the positive y axis at time 0,5,10,20,40. The maximum v-displacement always occurs at the end of the rupture zone. The displacement field decays exponentially with time. The relaxation effect is not obvious in this direction because our initial displacement is essentially perpendicular to this direction.

At the time of the earthquake very high shear stresses (about 110 bars) occur at the end of the rupture zone as shown in figure 6. The negative sign represents the orientation of the shear. These are dependent on the boundary conditions.

The time dependent solution of stress σ_x at dimensionless distances 0,4,8 along the x axis is shown in figure 7. For a 1.6 meter horizontal slip at the boundary,

the stress at x=0 is about 22.5 bars, which is consistent
with finite element calculations (Yang, 1979). The stess
decays exponentially with distance for short time inter-
vals after the earthquake disturbance. At several hun-
dreds of kilometer away from the boundary ,the relaxation
effect is again significant.

Figure 8 is the distribution of stress σ_x along the
y-axis. For short times, the stress σ_x changes sign
across the boundary of the rupture zone at y=800 km. A
sudden slip in the rupture zone increases the stress level
outside of the zone parallel to the plate boundary. This
slight increase in stress may trigger earthquakes in the
neighboring area along the plate boundary if the tectonic
stress level is already large.

3. Summary

Our two dimensional analytical study of stress propa-
gation has been completed. Although this is a simple two
layer model, it gives results that retain the significant
features found in more complicated finite element models.
It also provides some physical insight such as the time-
dependent exponential decay constant of the displacement
and stress fields and allow us to understand the process
in some detail. However, it is not easily generalized to
specific regions. Our future study will concentrate on

the development of an 'infinite element' based on our analytical solutions to simplify three dimensional finite element modelling.

REFERENCES

Christiansen, R. M., Theory of viscoelasticity an Intro-
duction, Academic Press, New York, 1971.

Delsemme,J., and Smith, A. T., Spectral analysis of earth-
quake migration in South America, pageoph 117,5,1979.

Dubner, H., and Abate, J., Numerical inversion of Laplace
transforms by relating them to the Finite Fourier
Cosine transform, Journal of the ACM, 15,1,1968.

Kasahara, K., Migration of crustal deformation, Tectono-
physics, 52, 329-341, 1979.

Mogi, K., Migration of seismic activity, Bull. Earthquake
Res. Inst. 46,53-74,1968a.

Mogi, K., Sequential occurrence of recent great earth-
quakes, J. Phys. Earth 16, 1, 30-36, 1968b.

Scholz, C. H., A physical interpretation of the Haicheng
earthquake prediction, Nature 267, 121-124,1977.

Yang, M., Time dependent tectonic deformation and stress
of lithosphere after earthquakes, EOS, Trans. Amer.
Geoph. Union, 60,number 18, p 316, 1979.

FIGURE 1

Finite two-dimensional plate model with length L,
width 2C, thickness of the lithosphere H1, and the
asthenosphreic thickness H2. The hatched area
represents the finite repture zone at the plate boun-
dary with width 2D. The x-coordinate is normal to
the plate boundary and the y-coordinate is parallel
to the plate boundary. The origin is located at the
center of the "fault". We apply a unit displacement
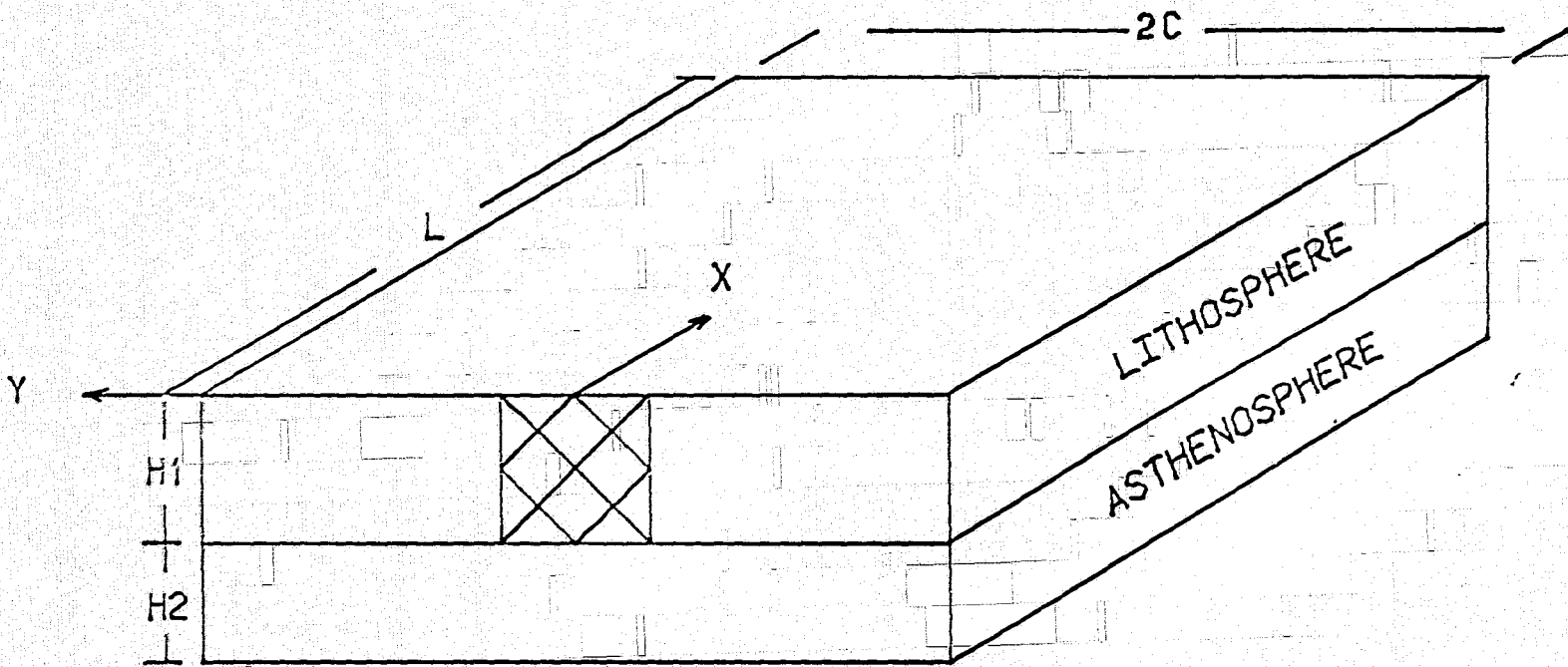throughout the thickness of the lithosphere in the
rupture zone to simulate an earthquake.

Figure 1

FIGURE 2

This is the top view of the model. A unit displacement in the rupture zone normal to the trench is applied to simulate earthquake slip. The rest of this boundary is fixed to the x-direction; however, motion in the y-direction is allowed. The ridge side is assumed to be stress free. Along the other two boundaries, we confine the motion to the y direction and ignore friction.

RIDGE

BASIC EQUATION : $H_1 \frac{\partial \sigma_x}{\partial x} = \sigma_{zx}$

EXTENDED TO PLANE STRESS PROBLEM

X

Y

TRENCH

BOUNDARY CONDITIONS :

1) UNIT X-DISPLACEMENT IN THE RUPTURE ZONE

2) RIDGE IS STRESS FREE

3) ZERO Y-DISPLACEMENT ON THE OTHER TWO BOUNDARIES.

Figure 2

FIGURE 3

The u-displacement parallel to the x axis. Distances are non-dimensionalized by the thickness of the lithosphere. The number by the curve is the dimensionless time. At time 0, the disturbance at plate boundary effects only adjacent regions. As time increases, it gradually propagates deeper into the plate.

FIGURE 4

The velocity (time derivative of the u-displacement) as a function of time along the x-axis at x=4,8,12. The effect of the asthenospheric stress relaxation is obvious. The maximum velocity at x=4 is about 25% smaller than the corresponding one dimensional case.
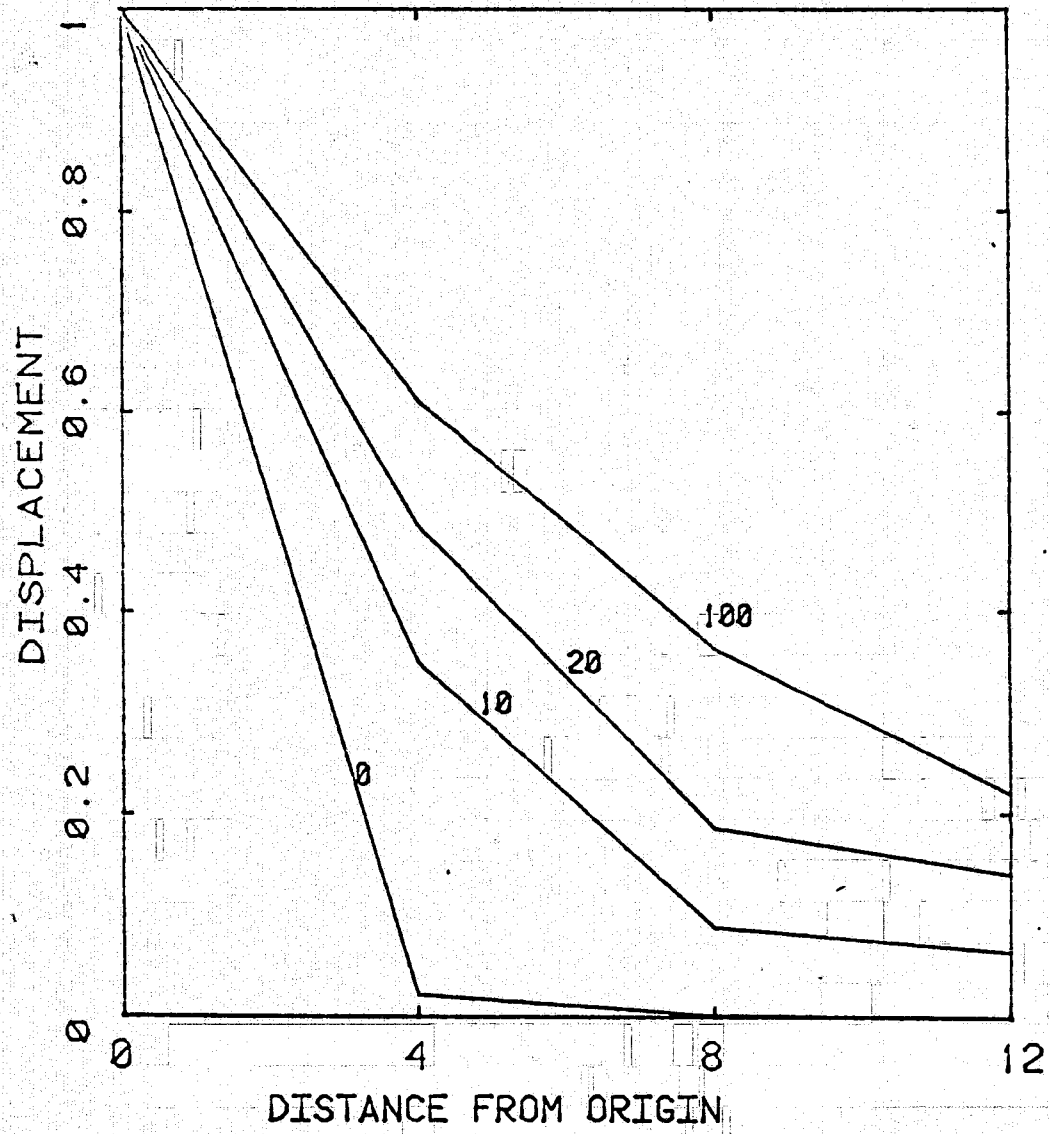
Figure 3

VELOCITY AT X-AXIS
TIME (YR)
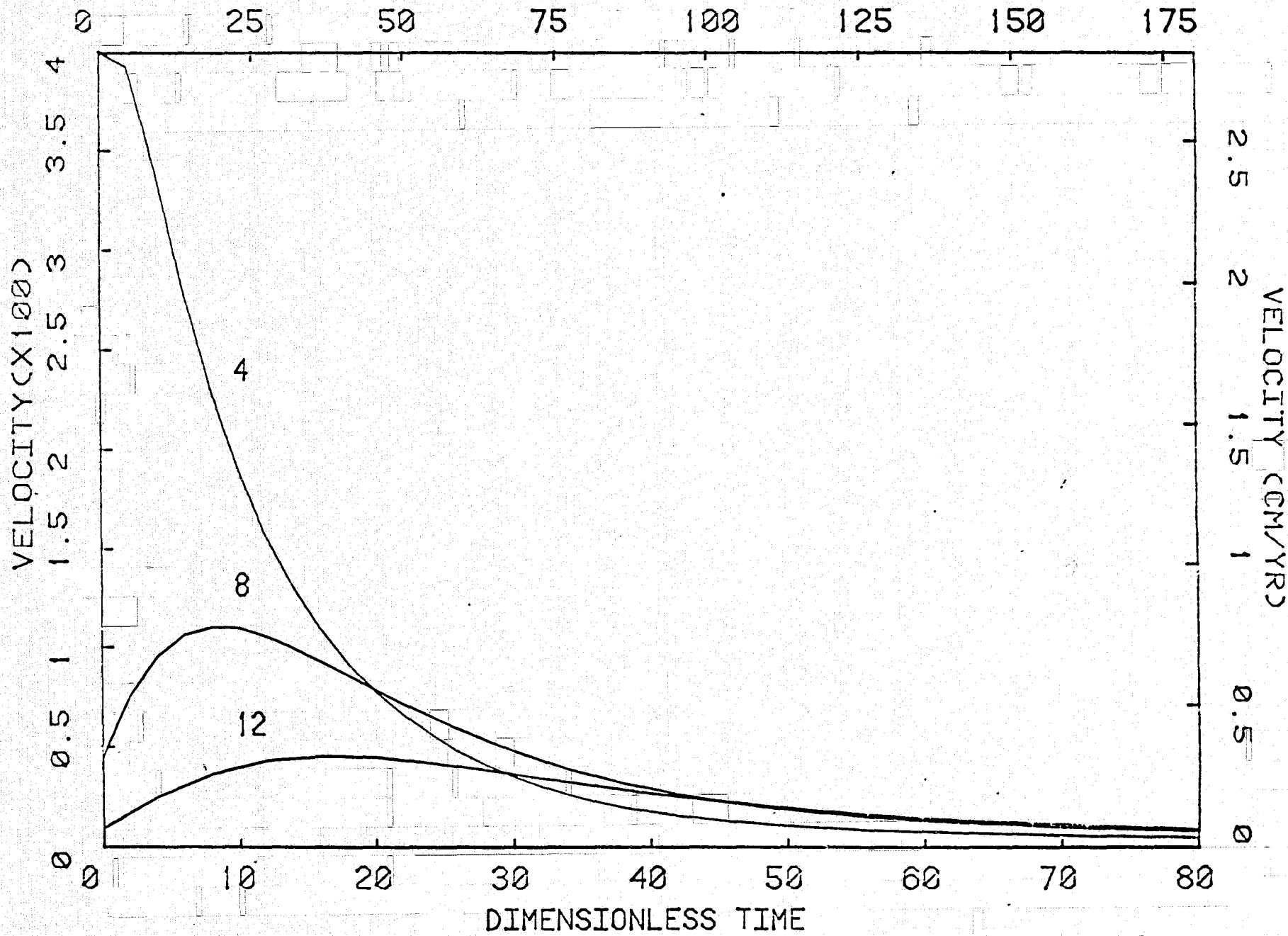
Figure 4

FIGURE 5

The v-displacement along the positive y direction at time 0,5,10,20,40. The maximum displacement occurs at the end of the rupture zone. Displacement decays rapidly at short time. The relaxation effect is not obvious in this direction because of the direction of initial conditions.

FIGURE 6

Shear stress along the positive y axis. The dimensional units is obtained using the parameters specified in the text. Very high shear stress occur at the end of the rupture zone. The negative sign represents the orientaiton of the shear.
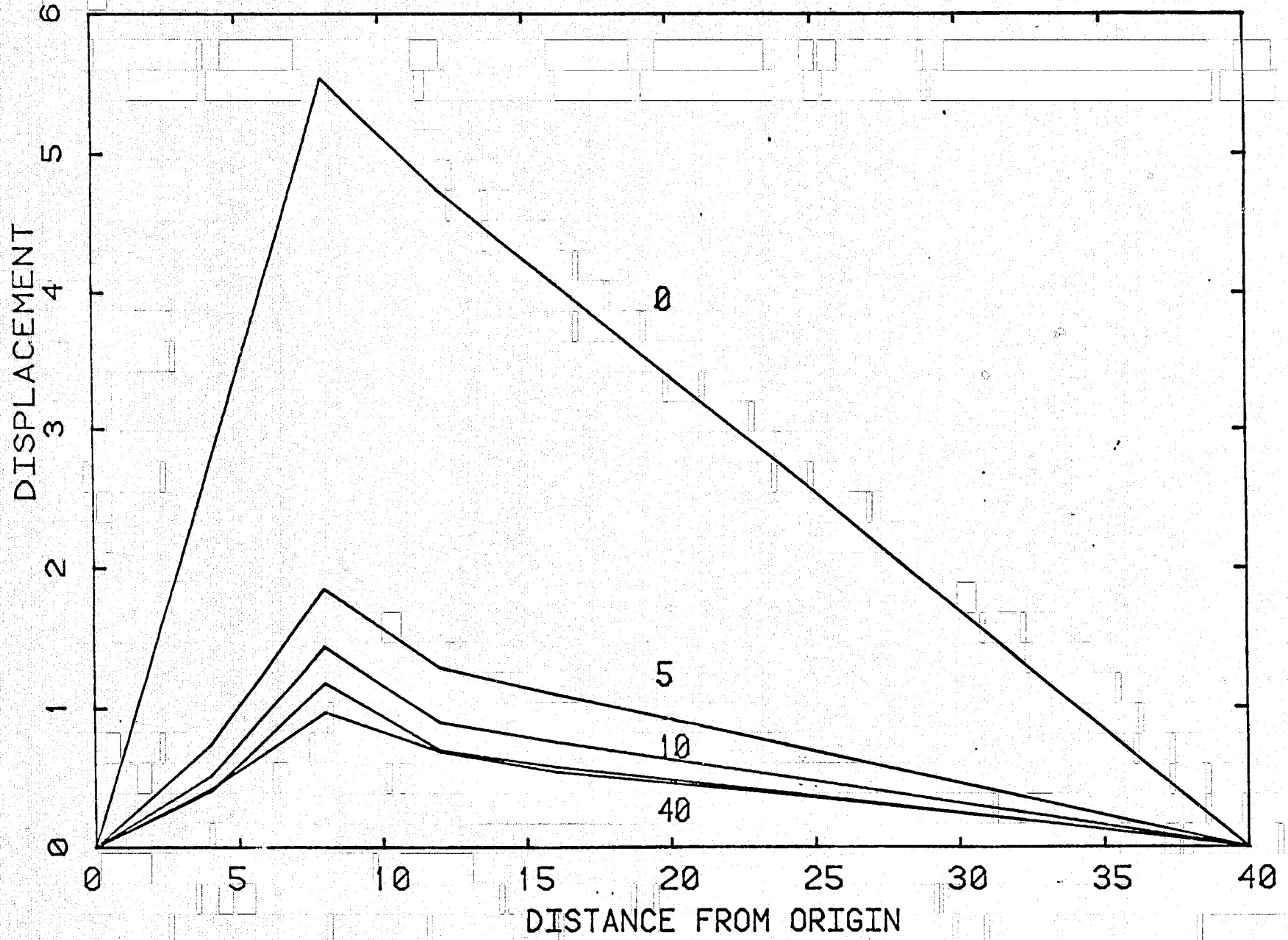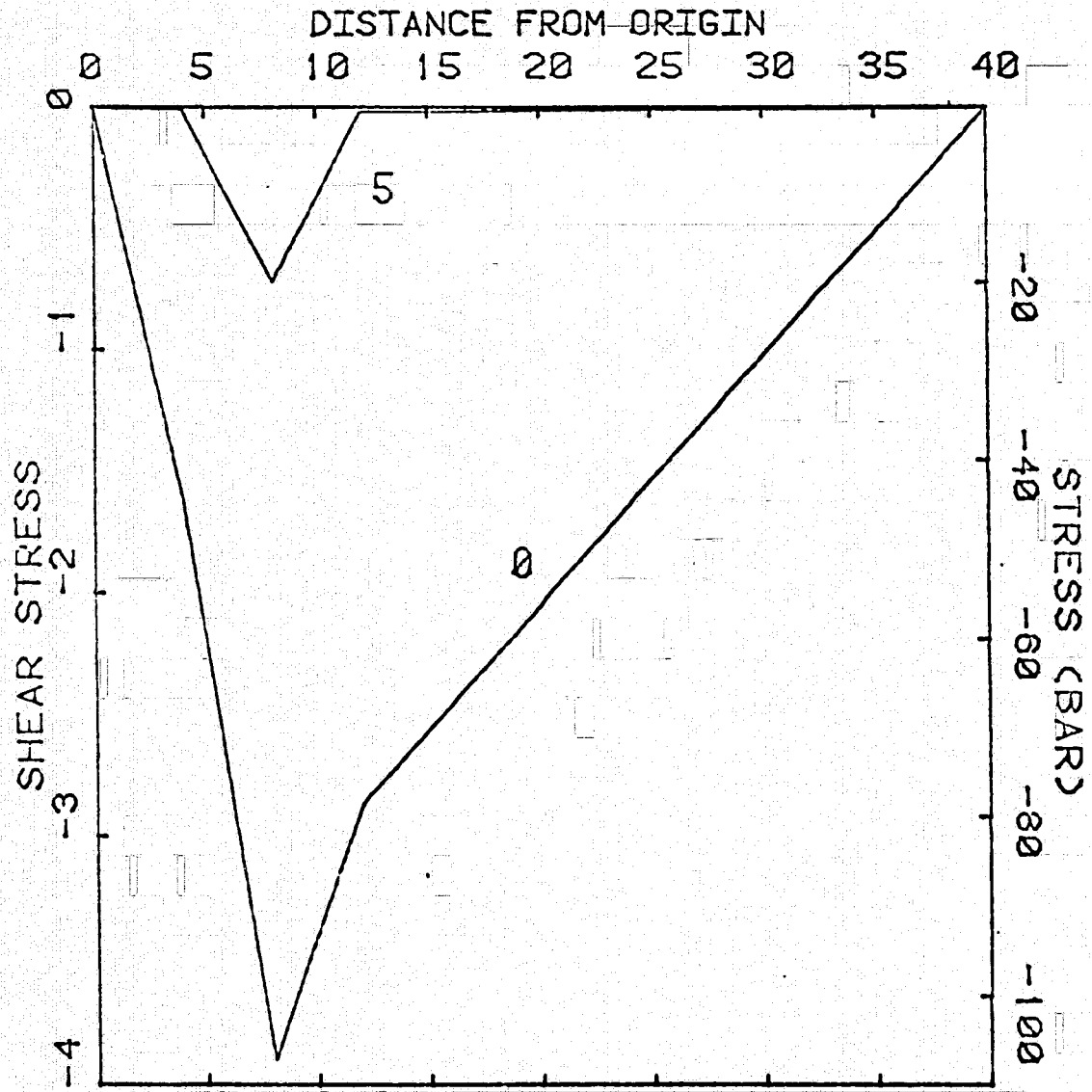
Figure 5

Figure 6

FIGURE 7

The stress σx at dimensionless distances 0,4,8 along the axis. For a 1.6 meter horizontal slip at the boundary, the maximum stress right behind the rupture zone is about 22.5 bars. At greater distances, the stress relaxation is significant.

FIGURE 8

Distribution of stress σx along the y axis. For short times, the stress changes sign across the boundary of the rupture zone. A slip in the negative x direction increases the compressional stress outside of the rupture zone parallel to the plate boundary. This might trigger earthquakes where the tectonic stress is already high.
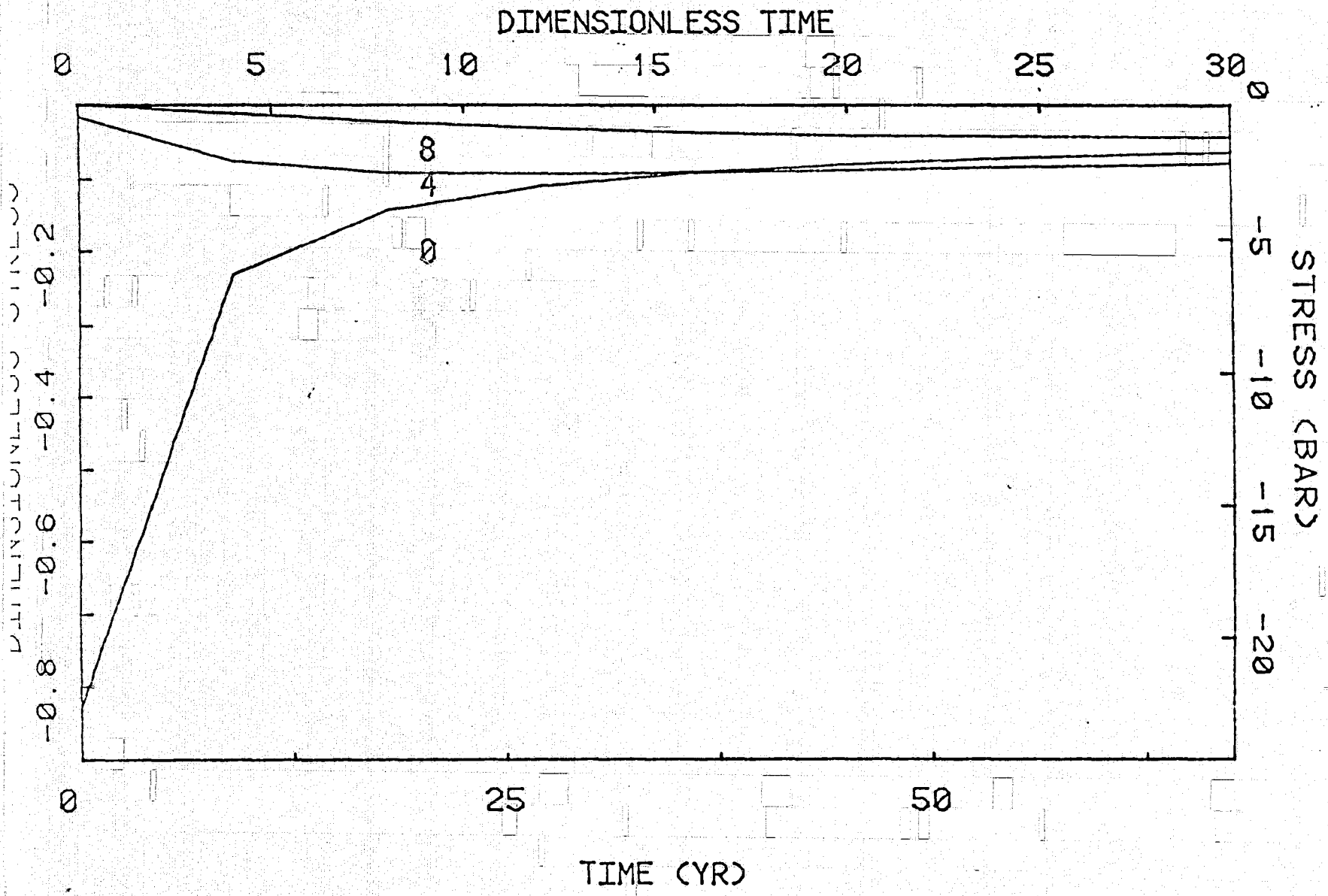
Figure 7
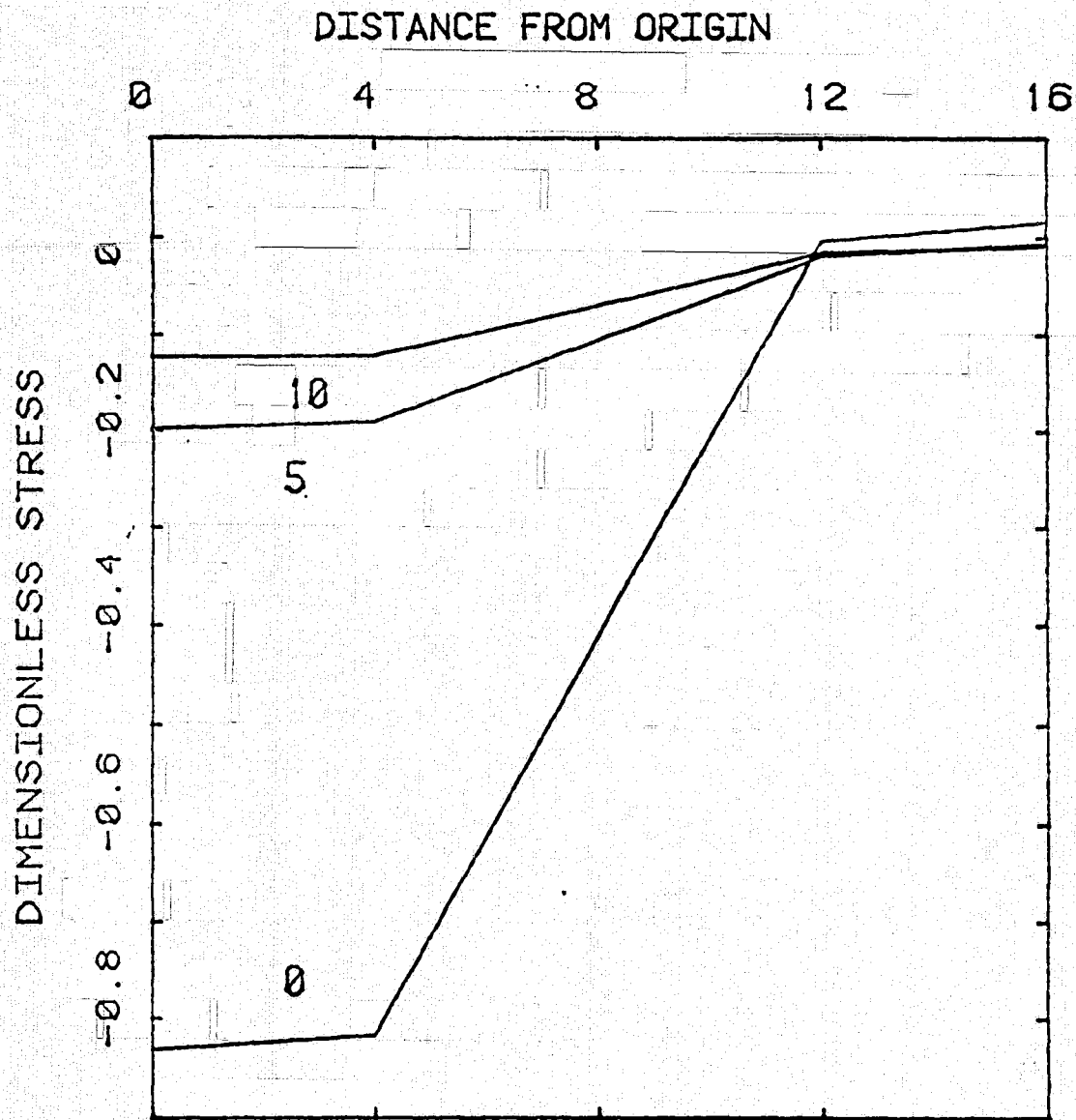
STRESS   X

DISTANCE FROM ORIGIN

Figure 8

PART 2:   TIME DEPENDENT DEFORMATION AND STRESS RELAXATION
AFTER STRIKE SLIP EARTHQUAKES

1.   INTRODUCTION

Great damage has been caused by shallow strike slip
earthquakes along plate boundaries in various parts of the
world. The mechanism of these earthquakes has long interested
seismologists. The study of geodetic measurements of the
1906 San Francisco earthquake led to the formulation of
elastic rebound theory (Reid, 1910), much of which has
remained a basic tenet on earthquake mechanism. The
continuous study of accumulation, release and relaxation
of stresses near the fault zone has provided a more detailed
mechanism of strike slip earthquakes (e.g. Chinnery, 1961;
Scholz and Fitch, 1969; Turcotte and Spence, 1974; Savage,
1975; Thatcher, 1975a,b; Budiansky and Amazigo, 1976; Rundle
and Jackson, 1977a,b; Savage and Prescott, 1978; Savage, 1979;
Thatcher, 1979; Turcotte et al., 1979). Much of the study
used geodetic measurements near the fault zone. In particular,
static elasticity and dislocation theory have often been applied
to the study.

Stress accumulation, release and relaxation are time
dependent phenomena. This is evident from geodetic data, the
migration behavior of earthquakes and asthenospheric viscosity.
In recent years, there have been intensive geodetic and creep
measurements in the San Andreas fault zone, and ultra precise
space technology has been applied to geodetic measurements
(e.g. Niell et al., 1979; Smith et al., 1979). Accurate

data will be available in the near future on the time
dependence of crustal deformation. A detailed, three-
dimensional time dependent model will be necessary for
interpretation of such data. On the other hand, earthquake
migration phenomenon have been observed along plate boundaries,
most noticeably along the North Anatolian fault (e.g. Mogi,
1968; Allen, 1969; Dewey, 1976; Toksöz et al., 1979).
Explaining this time dependent phenomenon also calls for
time dependent models.

. We calculated the long term time dependent response of
a set of models of strike slip events. The effect of
relaxation is isolated for the calculation. Most of the
previous attempts to model time dependent tectonic phenomenon
after earthquakes used two-dimensional models (e.g., Nur
and Mavko, 1974; Bischke, 1974; Smith, 1974; Savage and
Prescott, 1978; Thatcher and Rundle, 1979; Melosh and
Raefsky, 1979) or simple layer and half space solutions
(Rosenman and Singh, 1973a,b; Barker, 1976; Rundle and
Jackson, 1977a,b; Cohen, 1979; Cohen and Cook, 1979;
Lehner et al., 1979). Two-dimensional models assume
an infinite long fault, and the effects in the region beyond
the fault tip cannot be described. However, in this paper
we show that there are significant effects in the region
beyond the fault tip for strike slip events. Laterally
homogeneous models that assume no lateral heterogeneities
across the fault zone oversimplify the near-source problem.
Most data indicate the presence of lateral heterogeneities
near the fault.

In this paper, we present time dependent calculations
for finite strike-slip faults in laterally heterogeneous
media. We use the three-dimensional finite element method
to model strike slip events. The forward problem is set up
to predict time dependent deformation and stress after a strike
slip event for years and tens of years. The models are
chosen for representative earthquakes to show the characteristic
time dependent features of strike slip events. The boundaries
of inhomogeneities in the models are kept geometrically simple.
The model results indicate that geodetic measurements after
an event may provide information on rheological properties
near the fault zone which are vitally related to earthquake
occurrence.

II. MODEL DESCRIPTIONS

Fault Models

We present the computation for two classes of models, one
for a great earthquake, and the other for a moderate size
earthquake. Due to uncertainty in the viscosity structure,
several sets of viscosity values for the same fault model
are used to show a range of possible results. We are
interested in the general behavior of relaxation. No attempt
is made to model a specific region in detail. However, the
fault displacement and dimension for great earthquake models
(G1, G2 and G3) are comparable to those of the 1906 San
Francisco earthquake or the 1939 North Anatolian earthquake.
The dimension for fault models M1 and M2 are appropriate

for a magnitude 5.5-6.0 earthquake such as the Coyote Lake earthquake of 1979 (M = 5.7).

We model the strike slip earthquake as a sudden slip on two sides of a rectangular vertical fault surface. The offset values are prescribed, and the subsequent displacements and relaxation are computed. We assume that the slip on fault stops after the step function slip. This probably will happen if deviatoric tectonic stresses are relieved near the fault zone and friction again takes over, and the region deforms in a coherent manner. However, there may be cases where this condition is violated. Slow afterslip is sometimes observed after an earthquake (e.g., Burford, 1972; Buckham et al., 1977; Coppersmith et al., 1979). If afterslip does not last long relative to relaxation time (years) the long term effect will be similar to a step function.

The model region for models G1, G2 and G3 is 2740 km long, 2320 km wide and 700 km deep. The fault is a rectangle 350 km long and extends vertically from 0 to 40 km depth. The relative fault offset is 5 meters strike slip, except that near the edges of the fault area it tapers off. The offset tapers off linearly from 5 meters at 20 km depth to zero at 40 km depth, and it tapers off linearly to zero at 35 km from the tips along the strike direction as shown in Figure 1.

The model region for models M1 and M2 is 196 km long, 169 km wide and 80 km deep. The fault is a vertical

rectangle 20 km long and 12 km deep. The model earthquake has no surface rupture. It has relative offset of 30 cm from 3 to 9 km depth, and the offset tapers off linearly to zero from 9 to 12 km depth and 3 to 0 km depth. It also tapers off linearly to zero at 2.5 km from tips along the strike direction (Figure 2).

Material Properties

There is controversy over the laws governing creep behavior of earth material (Weertman, 1978). Linear Newtonian behavior of the mantle fits the post-glacial rebound data, but laboratory rock mechanics experiments show non-linear creep behavior. For calculation of perturbation caused by the earthquake, we choose the linear viscoelastic models, simply because viscoelastic material contains the essential elements of time dependent relaxation phenomena, while the assumption of linearity greatly simplifies the physical picture, as we can separate the effect of perturbations caused by the earthquake.

The material in the model is assumed to be elastic in bulk and maxwellian viscoelastic in distortion. The short term elastic constants of earth vary slowly in space (Hadden and Bullen, 1969). On the other hand, the viscosity value changes by orders of magnitude from lithosphere to asthenosphere (Cathles, 1975; Peltier and Andrews, 1976). The contribution

to viscoelastic relaxation due to changes in elastic parameters
is therefore relatively unimportant. In order that we do not
unnecessarily complicate the physical picture, we assume in
all the models that the elastic parameters are uniform in
the region, with bulk modulus 1.3×10^{12} dyne/cm^2 and Poisson's
ratio 0.25. The different model results will be due to
different viscosity structures in the models.

The viscosity of the earth is not a well constrained
quantity, especially near a tectonically active zone such
as a transform fault. The lithosphere in general can
withstand deviatoric stresses for a million years or longer.
The thickness of the elastic lithosphere in continental
regions is probably greater than 50 km. The asthenosphere
has a viscosity value orders of magnitude smaller than the
lithosphere. From analyses of post-glacial rebound data,
the low viscosity layer beneath the lithosphere can be on
the order of 10^{20} poise (Cathles, 1975; Peltier and Andrews,
1976). The low viscosity implies that deviatoric stresses
cannot be sustained there for a time scale larger than several
years to decades.

Near an active transform fault, where only shallow
earthquakes are observed suggests lateral heterogeneities.
For examples, in the San Andreas fault zone earthquakes are
usually shallower than 10 to 15 km, indicating that stress
is being relieved anelastically below this depth. This

thickness of the "seismo-genic" layer is simply too small
compared to the generally accepted lithospheric thickness,
suggesting that a low viscosity zone may exist under the
fault. Lachenbruch and Sass (1973, 1979) found that the
San Andreas fault system is contained in a broad zone of
high heat flow anomaly. They concluded that the thin
seismo-genic layer is more brittle than the layer beneath
it, implying the possibility of shallow low viscosity zone
there. Theoretically, the shearing motion should also cause
temperature and viscosity structure to vary laterally (Yuan
et al., 1978). Three dimensional inhomogeneities in elastic
parameters are also observed in tectonically active regions
(Zandt, 1978) although it is difficult to estimate viscosity
structures from elastic parameters.

There is little information on the viscosity in a
fault zone. Budiansky and Amazigo (1978) estimate the
"effective viscosity" of lithosphere to be 10^{21} poise in
California. Nur and Mavko (1974) and Smith (1974) analyzed
the vertical deformation of the 1946 Nankaido earthquake and
conclude the viscosity value below the elastic lithosphere is
on the order of 10^{19} to 10^{20} poise. Thatcher and Rundle (1979)
found that a viscosity value of about 5×10^{20} poise in the
asthenosphere near Japan fits geodetic measurements. It
is plausible that the shearing motion and higher temperature
in the fault zone make the viscosity lower than in its
adjacent regions. We will carry out calculations for a

range of viscosity values.

Great earthquake model G1 is the control model; a layered structure is assumed. The lithosphere extends to 80 km depth; it is given a viscosity value of 10^{25} poise from 0 to 40 km, and 10^{24} poise from 40 to 80 km depth. A low viscosity layer extends from 80 to 180 km depth, with a viscosity value of 10^{20} poise. Below 180 km, the mantle viscosity is assumed to be 10^{22} poise as shown in Figure 3.

More realistic models incorporate lateral heterogeneities across the fault. In model G2, a low viscosity zone rising to 20 km below the surface and extending 140 km on each side of the fault is assumed. The viscosity value is assumed to be 10^{20} poise, the same as in the low viscosity asthenosphere extending from 80 to 180 km depth. Calculations show that differences in resulting time dependent deformation and stress relaxation between model G1 and G2 are significant. Model G3 has properties intermediate between model 1 and 2, with the low viscosity layer extending to 40 km depth. For moderate earthquake models M1 and M2 we assume that under the fault the low viscosity zone extends to shallower depths. Far away from the fault, the lithosphere is 80 km thick. Both models assume that from 12 km to 46 km depth there is a low viscosity zone 40 km wide on each side of the fault; from 46 km to 80 km depth, it is 70 km wide as shown in

Figure 4. Fast relaxation time is assumed for model M1 (viscosity 10^{19} poise) to establish the maximum possible effect of relaxation. Model M2 assumes the low viscosity value to be 10^{20} poise.

Computational Scheme

We use three-dimensional time dependent finite element models to calculate time dependent motions following an earthquake. We combine the frontal solution technique (Irons, 1970) to the unified time stepping approach (Zienkiewicz and Cormeau, 1974) for a versatile and efficient solution scheme. The calculation scheme is described in Appendix A.

Due to symmetry of a vertical strike slip earthquake, only a quarter of the region is needed to be modelled in the numerical scheme. All the models in this study use 720 elements and 2982 degrees of freedom. The grid structure of moderate earthquake models is a scaled grid of great earthquake models. Figure 5 is the top view of the grid structure of both classes of models. The three-dimensional model is made up of seven identical grid surfaces. The element is in 8 node, 24 degrees of freedom hexahedron with 8 gaussian integration stations. Elements with 27 integration stations have been used on some models. The results are nearly identical with those of 8 integration stations.

Since only a quarter of the region is used in the numerical scheme, the boundary conditions must simulate those of the complete strike slip fault. The fault area is contained in the boundary plane $x = 0$ (Figure 5). The boundary plane $y = 0$ is a symmetry surface bisecting the physical fault model. On plane $y = 0$ the displacement in x direction is constrained; on plane $x = 0$ the displacement in y direction is constrained, except on the fault surface half the fault offset value is prescribed. The effect caused by the event decreases with distance from the fault. We choose a region large enough such that the artificial external boundary condition does not influence the behavior of the region we are interested in. We used rigid and free boundary conditions on the sides of the region. We present results only for those elements where resulting stresses differ by less than a few per cent for these two extreme cases. We used 12 time steps for models G1, G2 and G3 to calculate time dependent values for up to 49 years after the event. For thin lithosphere and fast relaxing models M1 and M2, we used 14 time steps for 9.5 years after the event.

III. Model Results

Great Earthquake Models

The results of time dependent deformation and stress from different models are presented and compared in this section. Model G1 is the control model with a laterally

homogeneous layered structure. The horizontal displacements
on free surface at selected locations for model Gl are
shown in Figure 6a. The four figures give the horizontal
displacements at time = 0, 9.5, 25 and 49 years after event,
respectively. The initial (time = 0) pattern is typical of a strike
slip fault in elastic media. Afterwards the displacement
gradually increases with time. The initial displacements
decrease very fast with distance from the fault. The
relaxation process spreads the deformation outward from
the fault zone.

In contrast with model Gl, model G2 has a low viscosity
zone extending to shallow depth near fault. The result of
horizontal displacement on free surface at selected locations
is given in Figure 6b. The instantaneous response is the
same as for model Gl, since they have the same elastic
parameters. However, the magnitude of time dependent
displacement is much larger and concentrated near the fault
zone (where the low viscosity zone is shallow). The time
dependent effects can be seen more clearly in Figures 7a
and 7b, where the displacements along the line perpendicular
to the center of fault (x axis in Figure 1) are shown. Near
the fault zone the time dependent deformation is in general
small compared to the instantaneous response for model Gl,
while the shallow low viscosity zone in model G2 significantly
increases the magnitude of time dependent displacement.

The contours of vertical displacement on free surface immediately after the event are shown in Figure 8a. Also shown (Fig. 8b) are the shear stress contours. The results are what we expect from a shallow strike slip event. In the vertical displacement figure there is subsidence in a broad area in the upper right quadrant, except near the fault tip. Our grid resolution cannot resolve the very small uplift zone near the fault tip, but the overall pattern is very similar to that of the analytic half space solution of Chinnery (1961). Subsequent time dependences show characteristic differences between layered and lateral inhomogeneous models. The contours of vertical displacement change after the event (total displacement minus instantaneous response) at 5 and 25 years after the event for model G1 and are given in Figures 9a and 9b. The results of model G2 are given in Figures 10a and 10b. On the upper right quadrant, for model G1 the time dependent vertical movement is continous subsidence near the fault zone, and uplift away from it. This result is expected if the horizontal displacement is spreading out from the near fault region. The magnitude of this vertical movement is on the order of several centimeters. In contrast, the results for model G2 is continuous uplift throughout the upper right quadrant. The physical reason for this difference can be seen from the horizontal displacement plots (Figures 6a and 6b). In the upper right quadrant in the figure, the "flow pattern" of the strike slip event is such that material

enters the near fault zone parallel to the strike direction, but leaves the fault zone in the direction 45 degrees from the strike direction at large distances. The low viscosity channel near the fault zone makes it easier for material to enter the fault zone; the thicker lithosphere beyond the low viscosity channel forms a barrier for material to fan out, thus material piles up near the fault zone and a bulge results. The uplift in model G2 is about 15 cm in 25 years. This effect is measurable by geodetic means, and could serve as a tool for investigating the viscosity structure of the fault zone.

Another interesting phenomenon is the time dependent character of the stress relaxation for these two different models. The instantaneous perturbation of horizontal shear stress component σ_{xy} at 10 km depth caused by the strike slip event is shown in Figure 8b, and σ_{xy} at 25 years later is shown in Figures 11a and 11b for models G1 and G2 respectively. Before the event, due to relative plate motion the stress component σ_{xy} should prevail near the fault zone. The earthquake relieves the prestress along the fault, but reenforces the prestress in front of the fault tip. More detailed time dependency can be seen in Figures 12a and 12b, where σ_{xy} vs. time at selected positions is shown. It can be seen that along the side of the fault, σ_{xy} is negative, implying the prestress is relieved. However,

viscoelastic relaxation in general accelerates the stress recovery. In front of the fault tip, σ_{xy} is positive, and the prestress is reenforced. This result of reenforcement of prestress has been considered to be the cause of secondary faulting (Chinnery, 1966) or creep and aftershocks in front of fault tip (Scholz et al., 1969). The earthquake may in time trigger subsequent events along the same fault. However, for the uniform thick lithosphere model G1, the time dependent stress is small compared to the instantaneous response, in this case subsequent earthquakes should happen immediately after the event rather than being delayed for years. Aftershocks located at the end of the main shock fit this picture, however, the short time delay of the aftershock is most likely due to local inhomogeneities and creep type relaxation rather than large scale mantle relaxation. On the other hand, for the laterally inhomogeneous model G2, a significant portion of the perturbing stress in front of fault tip is accumulated years after the event. The perturbing stress levels off a few decades after the event. This accelerated stress accumulation in front of the region of a strike slip fault makes the chance of earthquake happening greater during the several decades after the event. Triggered events can then happen years after the triggering event, as long as the stress diffusion is reenforcing the prestress. The earthquake sequence after the 1939 North

Anatolian event (Toksöz et al., 1979) is consistent with this stress diffusion mechanism.

It has been reported (Thatcher, 1975a) that the strain accumulation near the fault after the 1906 San Francisco event was episodic: the average strain rate parallel to the fault was about 2.5×10^{-6} per year for about 25 years after the event, and 0.6×10^{-6} per year afterwards. For model G1, the average strain rate at a point 18 km away from the fault is about 0.1×10^{-6} per year, much less than the observed value. The relaxation does not have an episodic behavior either. This simple model does not explain the 1906 data. For the laterally inhomogeneous model G2, the average strain rate at 18 km away from the fault is about 1.0×10^{-6} per year, similar to the observed values of the 1906 San Francisco earthquake. The tapering off of accelerated strain rate in about 30 years is also consistent with the San Francisco earthquake. The model is not a model of the San Francisco earthquake in detail, however, the results indicate that if the low viscosity extends to shallow depth under the fault, viscoelastic relaxation can contribute significantly to the time dependent deformation.

Model G3 has the low viscosity channel to 40 km depth instead of 20 km in model G2. The results are intermediate between G1 and G2. Figure 13 compares the contours of vertical displacement change at 25 years after the event for model G2 and G3. The result for model G3 in the upper

right quadrant is a broad region of uplift, and a small
region of slight subsidence near the fault tip. This
indicates that time dependent vertical displacement is
sensitive to the viscosity structure. Figure 14 compares
the shear stress σ_{xy} at selected positons vs. time for
models G2 and G3. There is accelerated strain rate a few
decades after the event for model G3, but the magnitude is
smaller than that of model G2.

Moderate Size Strike Slip Earthquake Models

Models M_1 and M_2 are models of moderate size earthquakes
with buried faults. Model M1 is the fast relaxation model,
with viscosity 10^{19} poise in the low viscosity zone, while
model M_2 uses viscosity 10^{20} poise instead. The horizontal
displacements at selected locations on free surface are
shown in Figures 15a and 15b. The results are generally a
gradual increase in magnitude. Figure 16 shows the
instantaneous response of vertical deformation on free
surface. In the upper right quadrant, there is a relatively
broad region of uplift near the fault, and subsidence far
away. This is expected for a fault with large fault depth
to length ratio (0.6 in this case). The vertical deformation
changes at 9.5 years later are given in Figures 17a and 17b.
For both models M1 and M2, in the upper right quadrant,
the vertical deformation is subsidence near the fault zone
and uplift far away from the fault, similar to that of the

layered medium case. This is probably because the width of the low viscosity channel is relatively large compared to the earthquake fault dimension. The magnitude of time dependent vertical deformation is small, generally less than 1 cm.

Figure 18 gives the time dependence of shear stress σ_{xy} at selected locations at 7.5 km depth. We again see the prestress is relieved along the fault, and reenforced in front of the fault. The time dependence is quite different for the two models: significant changes are completed within 5 years after the event for model M1, while the relaxation is linear in model M2 for the first decades. Though the magnitudes of quantities involved in those moderate earthquakes are of marginal use with the precision of present day available geodetic data, the result may be useful in conjunction with more precise and fast geodetic measurements in the future to infer the detailed structure near a fault zone.

IV. Discussion

In this study, we calculated time-dependent stress relaxation and deformation for large and moderate size earthquakes using different models. To compare these to observations we look at space-time migration of seismicity and to geodetic data. Migration of seismicity along plate boundaries has been observed in South America

(Kelleher, 1972), the West Pacific (Mogi, 1968), Alaska-Aleutian (Kelleher, 1970), the San Andreas Fault zone (e.g. Wood and Allen, 1973; Lee et al., 1979), and the North Anatolian fault zone (e.g. Richter, 1958; Mogi, 1968; Savage, 1971; Dewey, 1976; Toksöz et al., 1979). In the case of the North Anatolian faults there was a relatively quiescent period in seismicity prior to 1939. A bi-directional trend of seismic migration followed the great earthquake of 1939 (Toksöz et al., 1979). The occurrence of a sequence of events in rapid succession favors an accelerated stress accumulation process. In all the model results in section III, there is an accelerated stress accumulation process in the region in front of the fault tip. The magnitude of this accelerated stress accumulation is significant if a low viscosity zone under the fault extends to a depth of 40 km or less below the surface.

The possible scenario for the occurrence of a sequence of earthquake follows. The initial earthquake happens when stress accumulation exceeds the material strength. After this event, the stress accumulation accelerates in the region in front of the fault tip. The next earthquake happens when the combination of diffused stress and initial stress exceeds the strength; in turn this "triggered" earthquake triggers the next events in an adjacent region. The process continues until the stress along the whole fault zone is

relieved. This episode is then followed by a slow stress accumulation stage and relative quiescence in seismicity. Aftershocks that immediately follow the earthquake are probably due to local stress adjustments. Creep resulting from stress changes at the immediate vicinity of the source may result in relatively rapid stress adjustments in the source area. Migration of earthquakes in time may be related to viscoelastic relaxation and stress diffusion.

Time-dependent horizontal and vertical motions after a strike slip extent strongly depend on the viscosities under and near the fault zone. Although horizontal displacements are much larger than vertical, in this study we found that the time dependent behavior of vertical displacement is very sensitive to lateral heterogeneities of viscosity distribution. The bulge or subsidence formed after a great earthquake is of measureable magnitude. Thus levelling, in addition to horizontal geodetic measurements, after a great strike-slip earthquake will reveal the structure near the fault zone.

Deep aseismic slip below the seismo-genic layer is suspected of playing an important role in earthquake mechanism. Thatcher (1975a) reported accelerated strain rate decades prior to and after the 1906 San Francisco earthquake, and this can be explained by deep aseismic slip. Several studies have found that it is difficult to distinguish the effects of deep aseismic slip and viscoelastic relaxation from

geodetic measurements alone (Barker, 1976; Rundle and

Jackson, 1977a,b; Savage and Prescott, 1978). However,

this argument was based on calculations using laterally

homogeneous layered models and comparisons of the surface

deformation caused by viscoelastic relaxation and a certain

static dislocation at depth. As pointed out by Savage and

Prescott (1978), there are inherent difficulties in using

a simple layered model to compare the results, because in

such cases a distribution of slip at depth can always

duplicate the viscoelastic result. This inherent difficulty

may not arise if the symmetry is broken by three dimensional

inhomogeneity. The relaxation is more intensive near a

low viscosity zone, as we have shown in section III.

Although present day available geodetic data are not very

constraining, geodetic measurements in the future could

resolve this question.

A pre-seismic strain rate increase was reported in the

case of the 1906 San Francisco earthquake (Thatcher, 1975a).

This phenomenon cannot be caused by viscoelastic relaxation

alone, since relaxation is not a spontaneous process. However,

if viscosity is indeed low near the fault zone, relaxation

will add to the strain accumulation. A possible way

viscoelastic relaxation enters the accelerated strain rate

process could be a renforcement effect culminating in the

fracture of the seismo-genic layer; the aseismic slip at

depth increases the prestress on the locked fault, the effect of viscoelastic relaxation in general increases the deformation, so the prestress near the fault is further increased. The magnitude and relative importance of this positive reenforcement again depends on the viscosity near the fault.

In conclusion, we have implemented a versatile scheme to model the time dependent behavior after earthquakes. Non-uniform fault slip and three dimensional heterogeneities can be included in this scheme. The model results predict a stress diffusion phenomenon in front of fault tip after a strike slip event: if low viscosity extends to shallow depth near the fault zone, the shear stress in front of the fault tip will increase significantly with time. The time dependent deformation on free surface is more concentrated near the fault zone in that case than it is in the case of a laterally homogeneous layered structure. The time dependent behavior of vertical displacement near the fault may be completely altered by the presence of lateral inhomogeneities.

APPENDIX A

Time Dependent Finite Element Scheme Implementation

We combined the time stepping approach of Zienkiewicz and Cormeau (1974) and frontal solution of Irons (1970) for our finite element calculations. The central process of the frontal solution approach is the familiar Gaussian elimination. However, a global displacement-force equation is eliminated as soon as it has received all of the element and consistent nodal force contributions. The coefficients are moved to outside storage and other equations are updated accordingly. So only a small portion of the stiffness matrix will be in core at a time. This achieves the savings in core usage. Assembly and elimination processes are not separated. After completion of assembly and elimination, the coefficients are returned to core for back substitution in the order exactly opposite to which they were saved.

In the time stepping approach for time-dependent calculation the total strain ε is divided into three parts:

$$\varepsilon = \varepsilon^e + \varepsilon^{cp} + \varepsilon^o \tag{A-1}$$

where ε^e is the elastic strain, ε^o the initial strain and ε^{cp} the creep strain. Quite generally the constitutive law for creep strain rate and stress can be put into the form

$$\dot{\varepsilon}^{cp} = \Gamma \sigma \tag{A-2}$$

where dot indicates time rate. Γ is a symmetric matrix (may depend on stress) and σ is the stress.

The virtual work principle is

$$\int_\Omega \delta \varepsilon^T \sigma d\Omega - \int_\Omega \delta u^T b d\Omega - \int_{S_\sigma} \delta u^T t \, d S = 0 \tag{A-3}$$

where b is the prescribed body force, t the prescribed boundary traction, u the displacement, δ indicates variation and T indicates transpose. Integration is over the volume Ω and traction boundary s_σ respectively.

Let $\varepsilon = L\,u, \quad u = N\,a$ $\tag{A-4}$

L is the operator relating strain and displacement, N the shape function and a the nodal displacements. Then equation (A3) becomes

$$\delta a^T [\int_\Omega (L\,N)^T \sigma \, d\Omega - \int_\Omega N^T b \, d\Omega - \int_{S_\sigma} N^T t \, dS] = 0 \tag{A-5}$$

or $\quad \int B^T \sigma \, d\Omega - F = 0$

where $B = L\,N, \quad F = \int_\Omega N^T b \, d\Omega + \int_{S_\sigma} N^T t \, d S$

Using $\sigma = D\,\varepsilon^e = D\,(\varepsilon - \varepsilon^{cp} - \varepsilon^\circ)$, equation (A5) can be put into standard form $K\,a = V$ $\tag{A-6}$

where $K = \int_\Omega B^T D\,B \, d\Omega$

$$V = F + \int_\Omega B^T D\,\varepsilon^\circ \, d\Omega + \int_\Omega B^T D\,\varepsilon^{cp} \, d\Omega$$

Equation (A6) is the set of linear equations to be solved using frontal solution. ε^{cp} is obtained in time stepping fashion using equation $\dot{\varepsilon}^{cp} = \Gamma\sigma$. It can be shown that this procedure can be applied to the general visco-plastic problem (Zienkiewicz and Cormeau, 1974), including plasticity and creep problem as two extreme cases. The scheme can handle

nonlinear creep behavior as easy as linear material. However, nonlinear creep behavior depends on ambient

stresses, since the strain rate depends on the sum of ambient and perturbing stresses. In this paper we have assumed that linearity holds and treated only the perturbation caused by the earthquakes.

Acknowledgement

References

Allen, C.R., Active faulting in northern Turkey, Contr. No. 1577, Div. Geol. Sci., Calif. Inst. Tech., 32 p.

Barker, T.G., Quasi-static motion near the San Andreas fault zone, Geophys. J. R. astr. Soc., 45, 689-705, 1976.

Bischke, R.E., A model of convergent plate margins based on the recent tectonics of Shikoku, Japan, J. Geophys. Res., 79, 4845-4857, 1974.

Buckham, R.C., G. Plafker and R.V. Sharp, Surface faulting and afterslip along the Motagua fault in Guatemala, in Proc. Internat. Symp. on the Feb. 4th, 1976 Guatemalan Earthquake and the Reconstruction Process, vol. 1, 1978.

Budiansky, B. and J.C. Amazigo, Interaction of fault slip and lithosphere creep, J. Geophys. Res., 81, 4897-4900, 1976.

Burford, R.O., Continued slip on the Coyote Creek fault after the Borrego Mountain earthquake, in The Borrego Mountain Earthquake of April 9, 1968, U.S. Geol. Survey Prof. Paper 787, p. 105-111, 1972.

Cathles, L.M., The Viscosity of the Earth's Mantle, Princeton Univ. Press, 1975.

Chinnery, M.A., The deformation of the ground around surface faults, Bull. Seism. Soc. Am., 51, 355-372, 1961.

Chinnery, M.A., Secondary faulting, Canadian J. Earth Sciences, 3, 163-174, 1966.

Cohen, S.C., Postseismic viscoelastic surface deformation and stress, Part 1: Theoretical considerations, displacement and strain calculations, NASA Technical Memorandum 80292, Goddard Space Flight Center, Maryland, 1979.

Cohen, S.C. and G.R. Cook, Postseismic viscoelastic deformation
and stress, Part 2: Stress theory and computation,
dependence of displacement, strain and stress on fault
parameters, NASA Technical Memorandum 80334, Goddard Space
Flight Center, Maryland, 1979.

Coppersmith, K.J., T.H. Rogers and W.V. Savage, Ground cracks
and afterslip observed following the 6 August 1979 earthquake
at Coyote Lake, California, EOS, Trans. Am. Geophys. Un.,
60, 890, 1979.

Dewey, J.W., Seismicity of Northern Anatolia, Bull. Seism. Soc.
Am., 66, 843-868, 1976.

Haddon, R.A.W. and K.E. Bullen, An earth model incorporating free
earth oscillation data, Phys. Earth Planet. Int., 2, 35-49,
1969.

Irons, B.M., A frontal solution program for finite element
analysis, Int. J. Num. Meth. Eng., 2, 5-32, 1970.

Kelleher, J., Space-time seismicity of the Alaska-Aleutian seismic
zone, J. Geophys. Res., 75, 5745-5756, 1970.

Kelleher, J., Rupture zones of large South American earthquakes
and some predictions, J. Geophys. Res., 77, 2087-2103, 1972.

Lachenbruch, A.H. and J.H. Sass, Thermo-mechanical aspects of the
San Andreas fault system, in Proc. Conf. Tectonic Problems
of the San Andreas Fault System, ed. A. Nur and R. Kovach,
Stanford University Publications in the Geological Sciences,
13, 192-214, 1973.

Lachenbruch, A.H. and J.H. Sass, Heat flow and stress in the San Andreas fault zone, EOS, Trans. Am. Geophys. Un., 60, 955, 1979.

Lee, W.H.K., D.G. Herd, V. Cagnetti, W.H. Bakun and A. Rapport, A preliminary study of the Coyote Lake earthquake of August 6, 1979 and its major aftershocks, preprint, 1979.

Lehner, F.K., V. Li and J.R. Rice, Stress relaxation in the asthenosphere and rupture propagation along plate boundaries, EOS, Trans. Am. Geophys. Un., 60, 953, 1979.

Melosh, H.J. and A. Raefsky, Surface deformation due to vertical dip-slip faulting in a non-Newtonian earth, EOS, Trans. Am. Geophys. Un., 60, 316, 1979.

Mogi, K., Migration of seismic activity, Bull. Earthquake Res. Inst. Tokyo Univ., 46, 53-74, 1968.

Niell, A.E., K.M. Ong, P.F. MacDoran, G.M. Resch, D.D. Morabito, E.S. Claflin and J.F. Dracup, Comparison of a radio interferometric differential baseline measurement with conventional geodesy, Tectonophys., 52, 49-58, 1979.

Nur, A. and G. Mavko, Postseismic viscoelastic rebound, Science, 183, 204-206, 1974.

Peltier, W.R. and J.T. Andrews, Glacial-isostatic adjustment - I. The forward problem, Geophys. J. R. astr. Soc., 46, 605-646, 1976.

Reid, H.F., Permanent displacements of the ground, in The California Earthquake of April 18, 1906, Report of the State Earthquake Investigation Commission, Carnegie Institution of Washington, Washington, D.C. 1910.

Richter, C.F., Elementary Seismology, Freeman and Cooper, San

Francisco, p. 611-616, 1958.

Rosenman, M. and S.J. Singh, Quasistatic strains and tilts due to

faulting in a viscoelastic half-space, Bull. Seism. Soc. Am.,

63, 1737-1752, 1973a.

Rosenman, M. and S.J. Singh, Stress relaxation in a semi-infinite

viscoelastic earth model, Bull. Seism. Soc. Am., 63, 2145-

2154, 1973b.

Rundle, J.B. and D.D. Jackson, A three-dimensional viscoelastic

model of a strike-slip fault, Geophys. J. R. astr. Soc., 49,

575-591, 1977a.

Rundle, J.B. and D.D. Jackson, A kinematic viscoelastic model

of the San Francisco earthquake of 1906, Geophys. J. R. astr.

Soc., 50, 441-458, 1977b.

Savage, J.C., A theory of creep waves propagating along a

transform fault, J. Geophys. Res., 76, 1954-1966, 1971.

Savage, J.C., Comment on 'An analysis of strain accumulation on

a strike-slip fault', by D.L. Turcotte and D.A. Spence,

J. Geophys. Res., 80, 4111-4114, 1975.

Savage, J.C., Dislocation in seismology, in Dislocation Theory:

A Treatise, ed. F.R.N. NAbarro, N. Holland, Amsterdam, 1979.

Savage, J.C. and W.A. Prescott, Asthenosphere readjustment and

the earthquake cycle, J. Geophys. Res., 83, 3369, 1978.

Scholz, C.H., M. Wyss and S.W. Smith, Displacement on seismic

and aseismic slip on the San Andreas fault, J. Geophys. Res.,

74, 2049-2069, 1969.

Scholz, C.H. and T.J. Fitch, Strain accumulation along the San

Andreas Fault, J. Geophys. Res., 74, 6649-6666, 1969.

Smith, A.T., Time dependent strain accumulation and release at
island arcs: Implications for the 1946 Nankaido earthquake,
Ph.D. Thesis, M.I.T., Cambridge, Mass., 1974.

Smith, D.E., R. Kolenkiewicz, P.J. Dunn and M.H. Torrence, The
measurement of fault motion by satellite laser ranging,
Tectonophys., 52, 59-67, 1979.

Toksöz, M.N., A.F. Shakal and A.J. Michael, Space-time migration
of earthquakes along the North Anatolian fault zone and
seismic gaps, Pageoph, 117, 1158-1170, 1979.

Thatcher, W., Strain accumulation and release mechanism of the
1906 San Francisco earthquake, J. Geophys. Res., 80, 4862-
4872, 1975a.

Thatcher, W., Strain accumulation on the northern San Andreas
fault zone since 1906, J. Geophys. Res., 80, 4873-4880, 1975b.

Thatcher, W., Systematic inversion of geodetic data in Central
California, J. Geophys. Res., 84, 2283-2295, 1979.

Thatcher, W. and J.B. Rundle, A model for the earthquake cycle
in underthrust zones, J. Geophys. Res., 84, 5540-5555, 1979.

Turcotte, D.L. and D.A. Spence, An analysis of strain accumulation
on a strike-slip fault, J. Geophys. Res., 79, 4407-4412, 1974.

Turcotte, D.L., R.T. Clancy, D.A. Spence and F.H. Kulhawy,
Mechanisms for the accumulation and release of stress
on the San Andreas fault, J. Geophys. Res., 84, 2273-2282,
1979.

Weertman, J., Creep laws for the mantle of the earth, _Phil._ _Trans. R. Soc. Lond._, _A_, _288_, 9-26, 1978.

Wood, M.D. and S.S. Allen, Recurrence of seismic migration along the central California segment of the San Andreas fault system, _Nature_, _244_, 213-215, 1973.

Yuen, D.A., L. Fleitout and G. Schubert, Shear deformation zones along major transform faults and subducting slabs, _Geophys._ _J. R. astr. Soc._, _54_, 93-119, 1978.

Zandt, G., Study of three-dimensional heterogeneity beneath seismic arrays in Central California and Yellowstone, Wyoming, Ph.D. Thesis, M.I.T., Cambridge, Mass., 1978.

Zienkiewicz, O.C. and I.C. Cormeau, Viscoplasticity-plasticity and creep in elastic solids - a unified numerical solution approach, _Int. J. Num. Meth. Engr._, _8_, 821-845, 1974.

Figure Captions

Fig. 1. Fault for models Gl, G2, and G3.

(a) Schematic diagrams of fault, double hatched

area has maximum fault slip, single hatched area

has tapered fault slip.

(b) Fault slip along strike direction (Y direction).

(c) Fault slip vs. depth (Z direction).

Fig. 2. Fault for models M1 and M2

(a) Schematic diagram of fault, double hatched area has

maximum fault slip, single hatched area has tapered

fault slip.

(b) Fault slip along strike direction (Y direction).

(c) Fault slip vs. depth (Z direction).

Fig. 3. Sectional views of viscosity distribution for models (a) Gl,

(b) G2, (c) G3. Numbers with exponent are viscosity in poise.

Fig. 4. Sectional view of viscosity distribution for model

M1. Model M2 has the same structure except that the

viscosity is 10^{20} poise in low viscosity zone.

Fig. 5. Top view of the finite element grid. The three

dimensional model is made of seven identical plane grids.

Fig. 6. (a) Horizontal displacements on free surface due to

strike slip event in model Gl at 0, 9.5, 25 and 49

years after the event. The location of the fault is

indicated by a thick line segment and sense of motion

is indicated by a pair of arrows.

Dots are the locations where displacements are
calculated. Displacement is indicated by a line
segment from the dot. A scale for the displacement
(100 cm) and a scale for the map (400 km) are also
shown in the figure.

(b) The same plot for model G2.

Fig. 7. (a) Horizontal displacement vs. time along the line
perpendicular to the center of fault (x axis) on free
surface for model G1. The distance from the center of
the fault for points 1, 2, 3, 4, 5, 6 and 7 are 35, 70,
105, 140, 210 and 280 km. Schematic diagram of the
locations are shown at the bottom of the graph.

(b) The same plot for model G2.

Fig. 8. (a) Contours of vertical displacement on free surface
immediately after event for great earthquake models
G1, G2, and G3. Broken lines (negative values) indicate
subsidence; solid lines (positive values) indicate uplift.
The location of fault is indicated by a thick line segment
and a pair of arrows. The numbers near the contours are
uplift or subsidence in mm. The tick marks on the
frame are at half fault length interval (175 km). The
elastic response is the same for model G1, G2, and G3.

(b) Contours of shear stress component σ_{xy} at 10 km
depth immediately after the event for models G1, G2, and

G3. The numbers near the contours are stress in bars.
Stress concentrations are placed near fault tips from
interpolation, the actual grid resolution is 1/10 of
the fault length.

Fig. 9. (a) The vertical displacement on free surface at
5 years after the event minus the elastic response for
model G1. Numbers are amount of uplift or subsidence
in mm. Ticks are at half fault length intervals.
(b) The same plot at 25 years after the event.

Fig. 10. (a) Vertical displacement on free surface at 5
years after the event minus the elastic response for
model G2.
(b) The same plot at 25 years after the event.

Fig. 11. (a) Contours of shear stress component σ_{xy} at 10 km
depth 25 years after the event for model G1.
(b) Same plot for model G2.

Fig. 12. (a) Shear stress component σ_{xy} vs. time at selected
locations for model G1. The locations are at 10 km depth.
A schematic diagram indicating the horizontal positions
relative to the fault is given to the right of the
figure. The distances from the fault center along the
strike direction for points 1, 2, 3, 4, 5, 6, 7, 8, and
9 are 18, 53, 88, 123, 193, 228, 263, 307 and 385 km.
The distance from the fault perpendicular to the strike
direction is 35 km for point 9, 18 km for the rest of
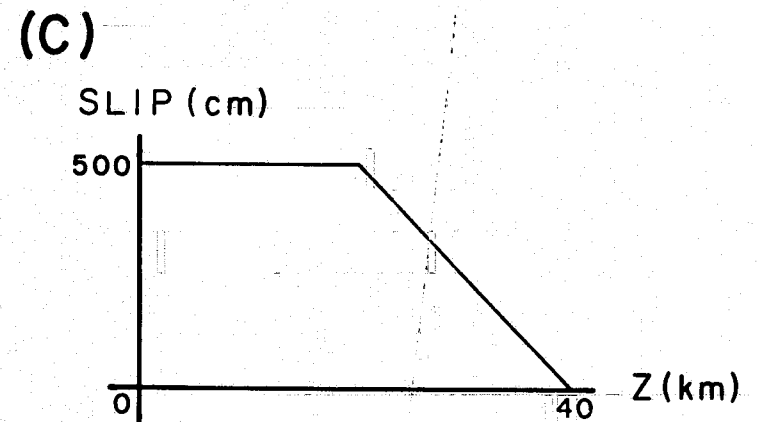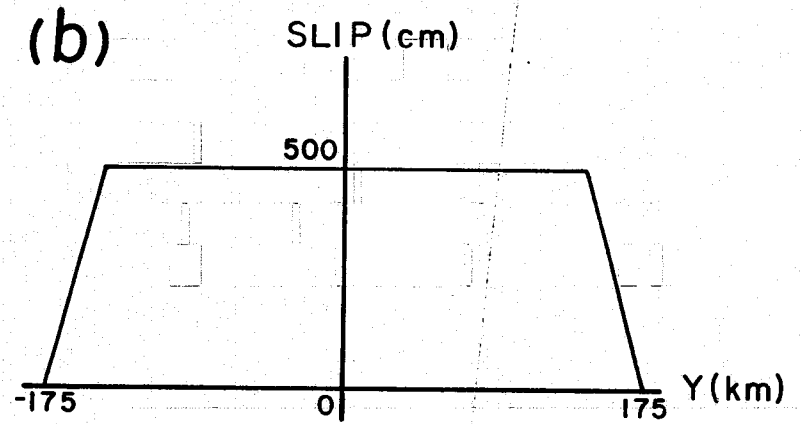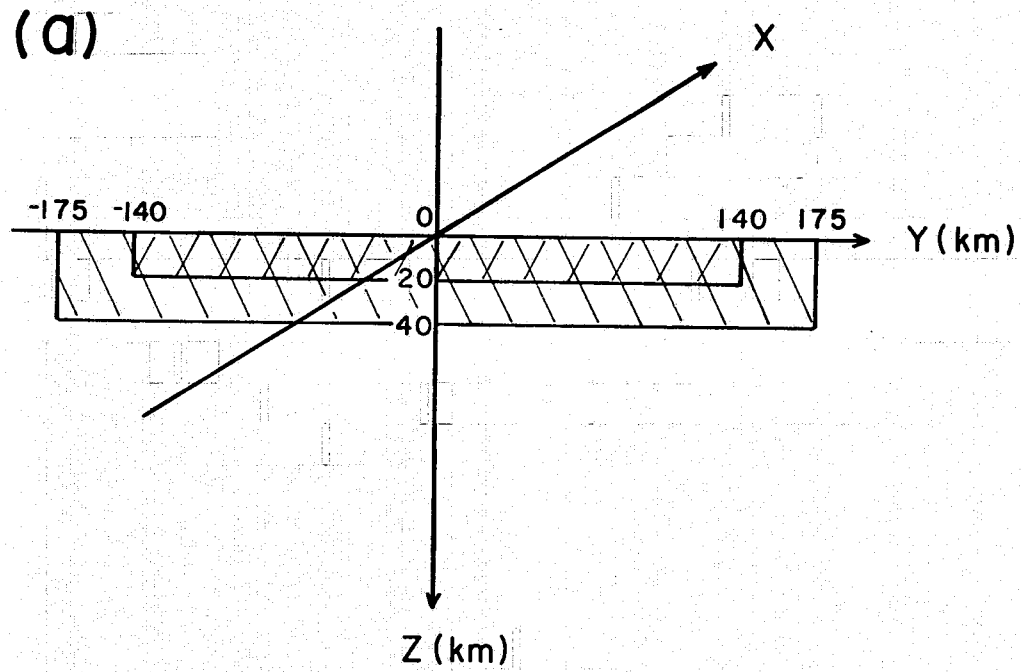the points.
(b) Same plot for model G2.

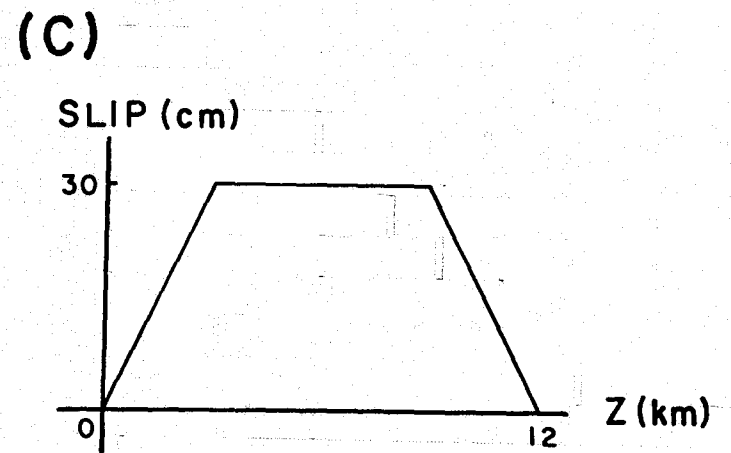Fig. 13.   (a) Contour of vertical displacement on free surface

at 25 years after the event minus the elastic response

for model G2 (Identical to figure 10b, included for

comparison).

(b) The same plot for model G3.

Fig. 14.   (a) Shear stress component σ_{xy} vs. time at

selected locations for model G2.   The locations are

at 10 km depth.   A schematic diagram indicating the

horizontal positions relative to the fault is given to

the right of the graph (identical to figure 12b, included

for comparison).

(b) The same plot for model G3.

Fig. 15.   (a) Horizontal displacements on free surface due

to strike slip event in model M1 at 0, 1, 3 and 9.5 years

after the event.

(b) The same plot for model M2.

Fig. 16.   Vertical deformation on free surface immediately

after the event for models M1 and M2.   Ticks are at

half fault length interval (10 km).   Numbers near the

contours are uplift (positive values) or subsidence

(negative values) in mm.

Fig. 17.   (a) The vertical displacement on free surface at

9.5 years after the event minus the elastic response

for model M1.   Numbers are uplift or subsidence in

mm.   Ticks are at half fault length interval (10 km).

(b) The same plot for model M2.

Fig. 18.   (a) Shear stress component σ_{xy} vs. time at selected

locations for model M1.   The locations are at 7.5 km

depth.   A schematic diagram indicating the horizontal

positions relative to the fault is given to the right

of the figure.   The distance from the fault center along

the strike direction for points 1, 2, 3, 4, 5, 6, 7, 8, 9

and 10 is 1.3, 3.8, 6.3, 11.3, 13.8, 16.3, 18.8, 21.9,

27.5 and 33.8 km.   The distance from the fault perpendicular

to the strike direction is 3.8 km for point 9 and 10, and

1.3 km for the rest of the points.

(b) The same plot for model M2.

Fig. 1

(a)

X

Y (km)

-10 -7.5   0   7.5 10

3

9

12

Z (km)

(b) SLIP (cm)

30

-10   0   10   Y (km)

(C) SLIP (cm)

30

0   12   Z (km)

Fig. 2

Fig. 3

Fig. 4

Fig. 5

(a)

0 YEARS   9.5 YEARS

25 YEARS   49 YEARS

0   400 KM   0   100 CM

(b)

0 YEARS   9.5 YEARS

25 YEARS   49 YEARS

0   400 KM   0   100 CM

Fig. 6

Fig. 7

O YEARS

(a)

VERTICAL DISPLACEMENT

O YEARS

(b)

SHEAR STRESS

Fig. 8

5 YEARS

(a)

25 YEARS

(b)

MODEL GI   VERT DISP CHANGE

MODEL GI   VERT DISP CHANGE

Fig. 9

5 YEARS

(a)

-5

-10

-25

-50

Y

5

10

25

50

X

50

25

10

-50

-25

-10

5

-5

MODEL G2   VERT DISP CHANGE

.25 YEARS

(b)

-10

-25

-50

-150

Y

10

25

50

150

X

150

50

25

-150

-50

-25

10

-10

MODEL G2   VERT DISP CHANGE

Fig. 10

(a) 25 YEARS

MODEL G1   SHEAR STRESS

(b) 25 YEARS

MODEL G2   SHEAR STRESS

Fig. 11

Fig. 12

(a)

(b)
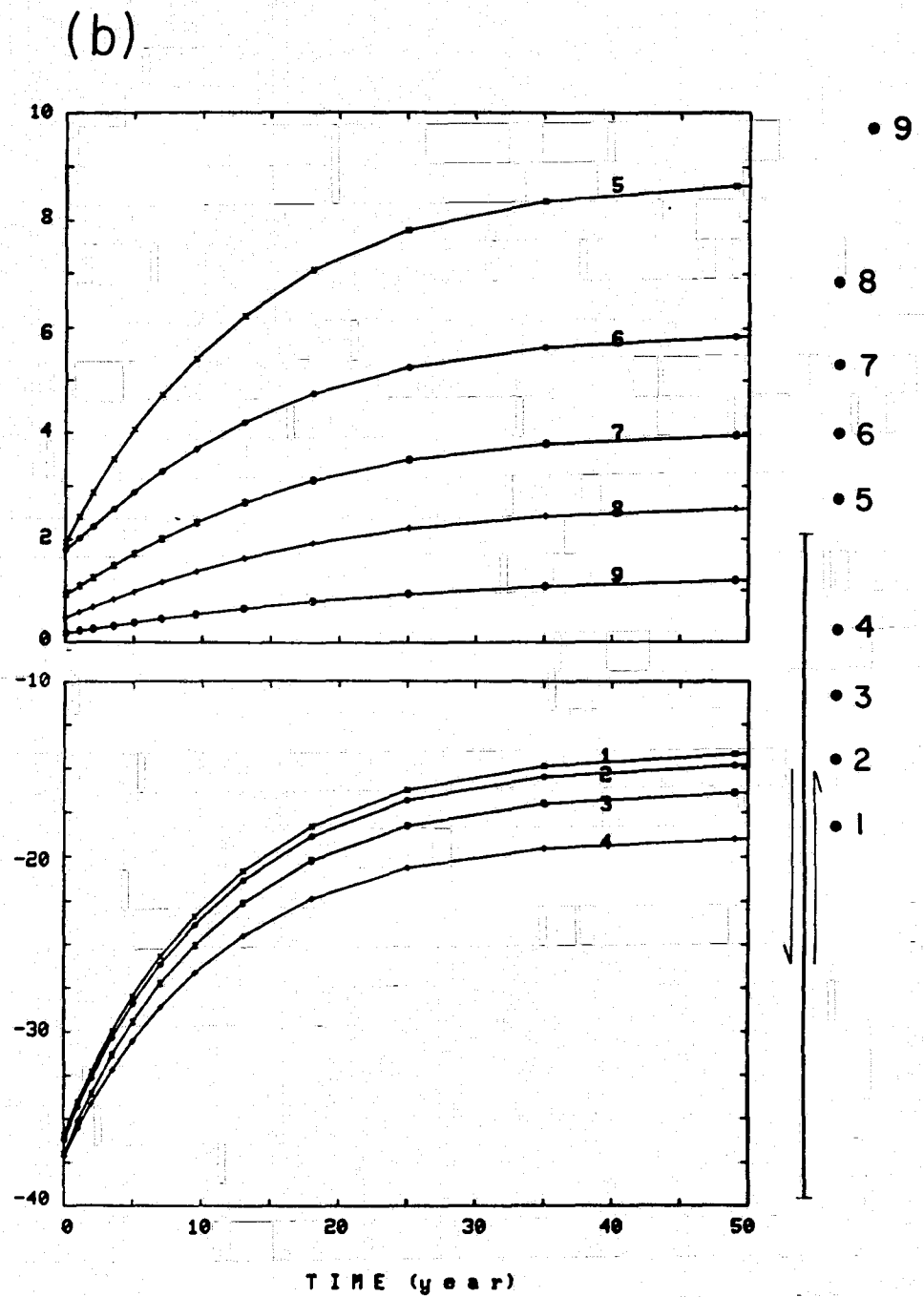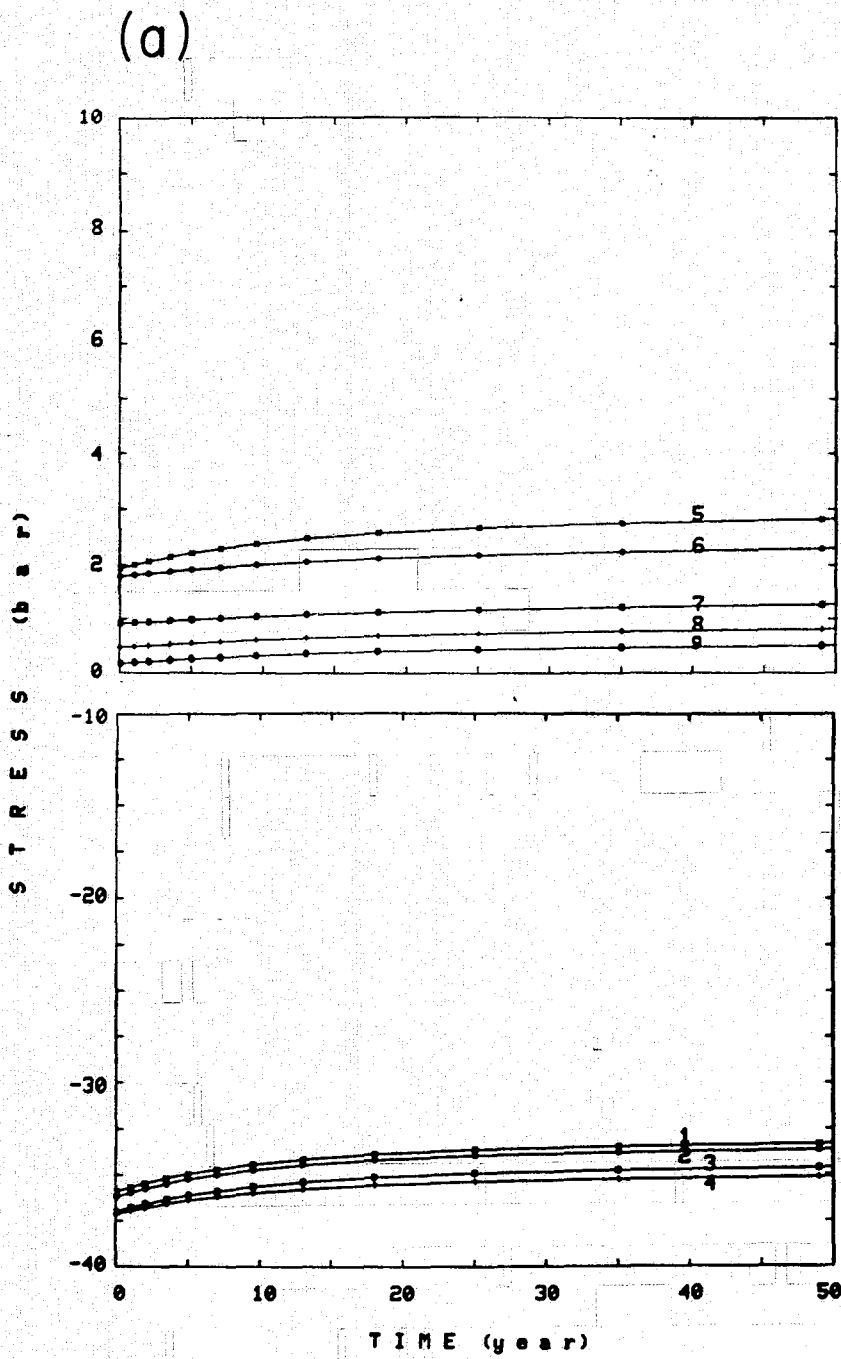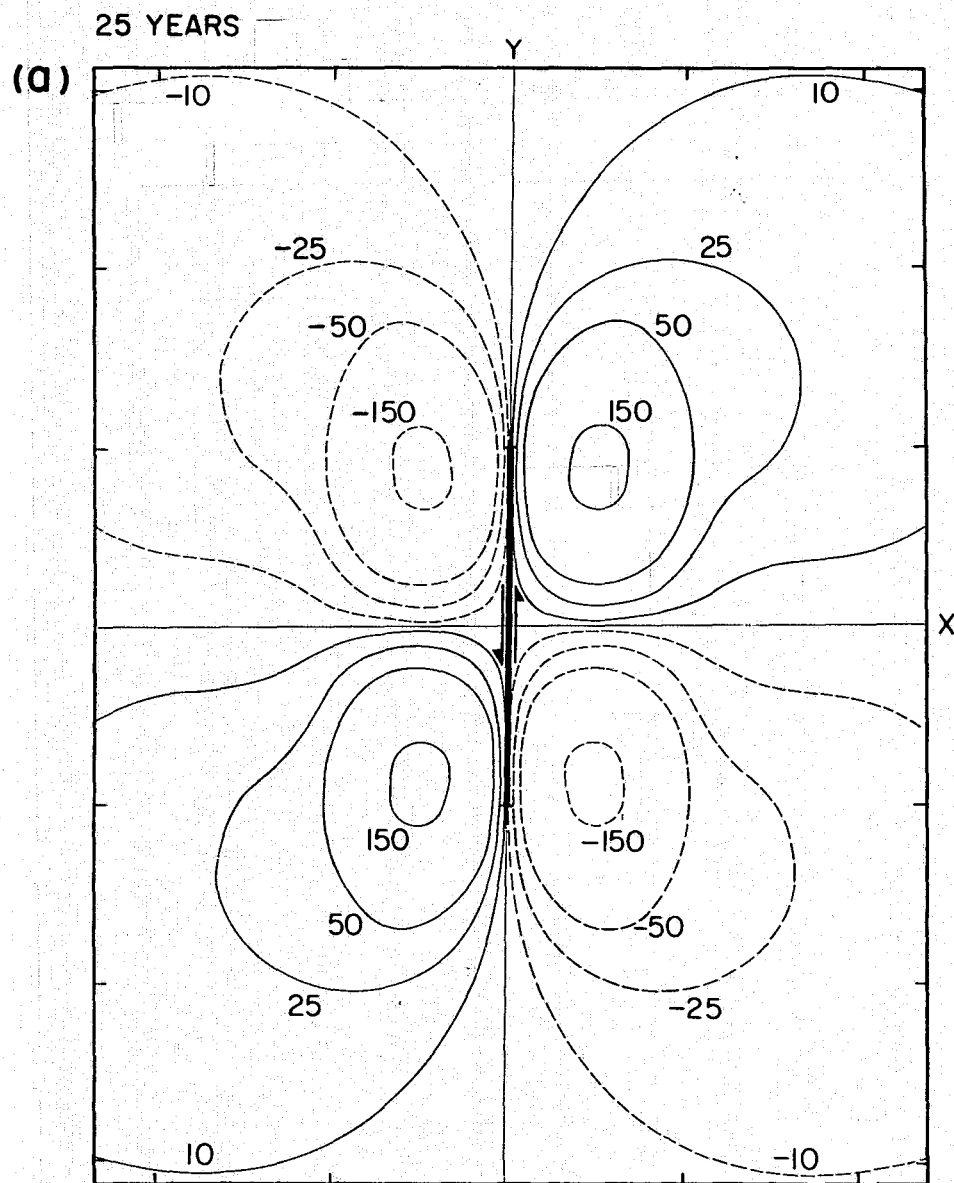
MODEL G2   VERT DISP CHANGE
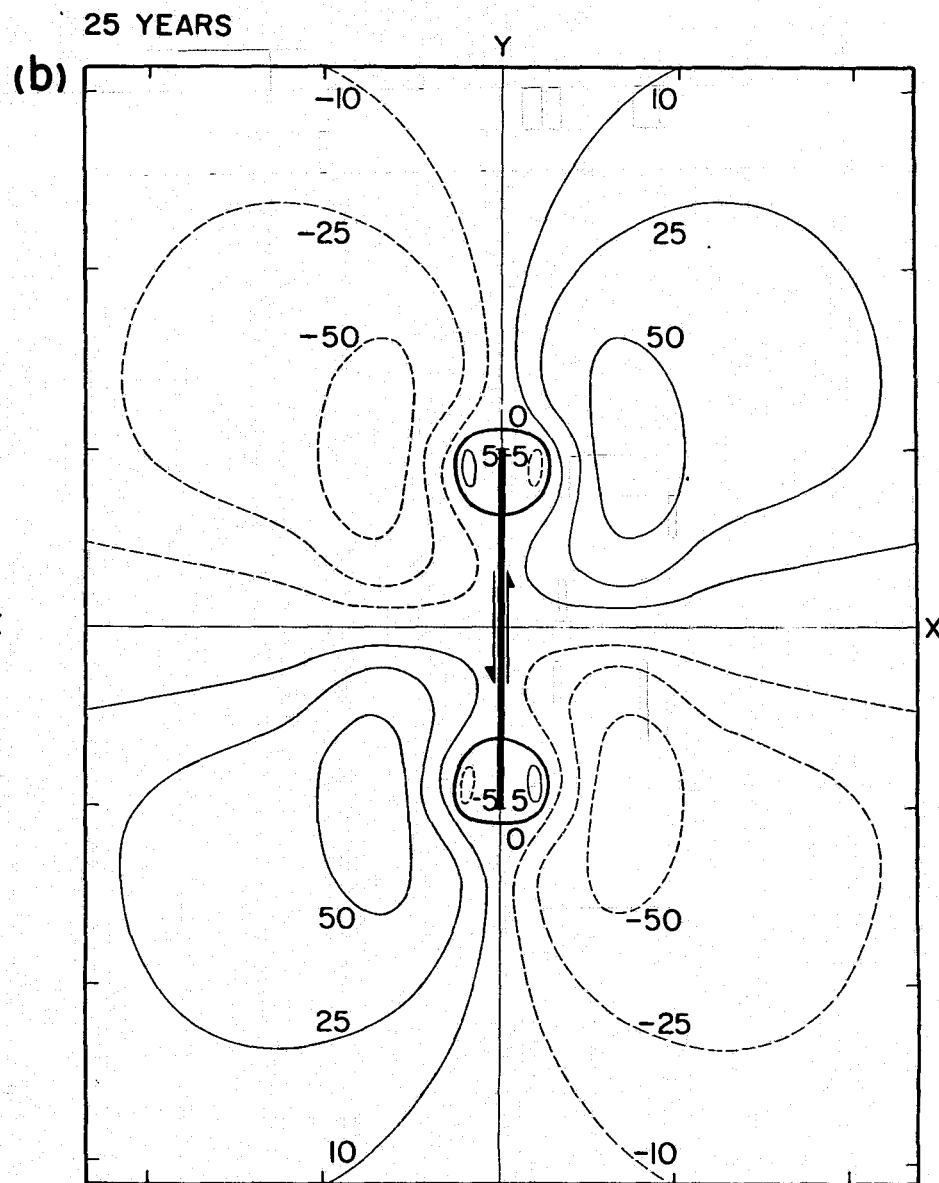
MODEL G3   VERT DISP CHANGE

Fig. 13

Fig. 14

(a)

O YEARS   I YEAR

3 YEARS   9.5 YEARS

0 20 km   0 60 mm

(b)

O YEARS   I YEAR

3 YEARS   9.5 YEARS

0 20 km   0 60 mm

Fig. 15
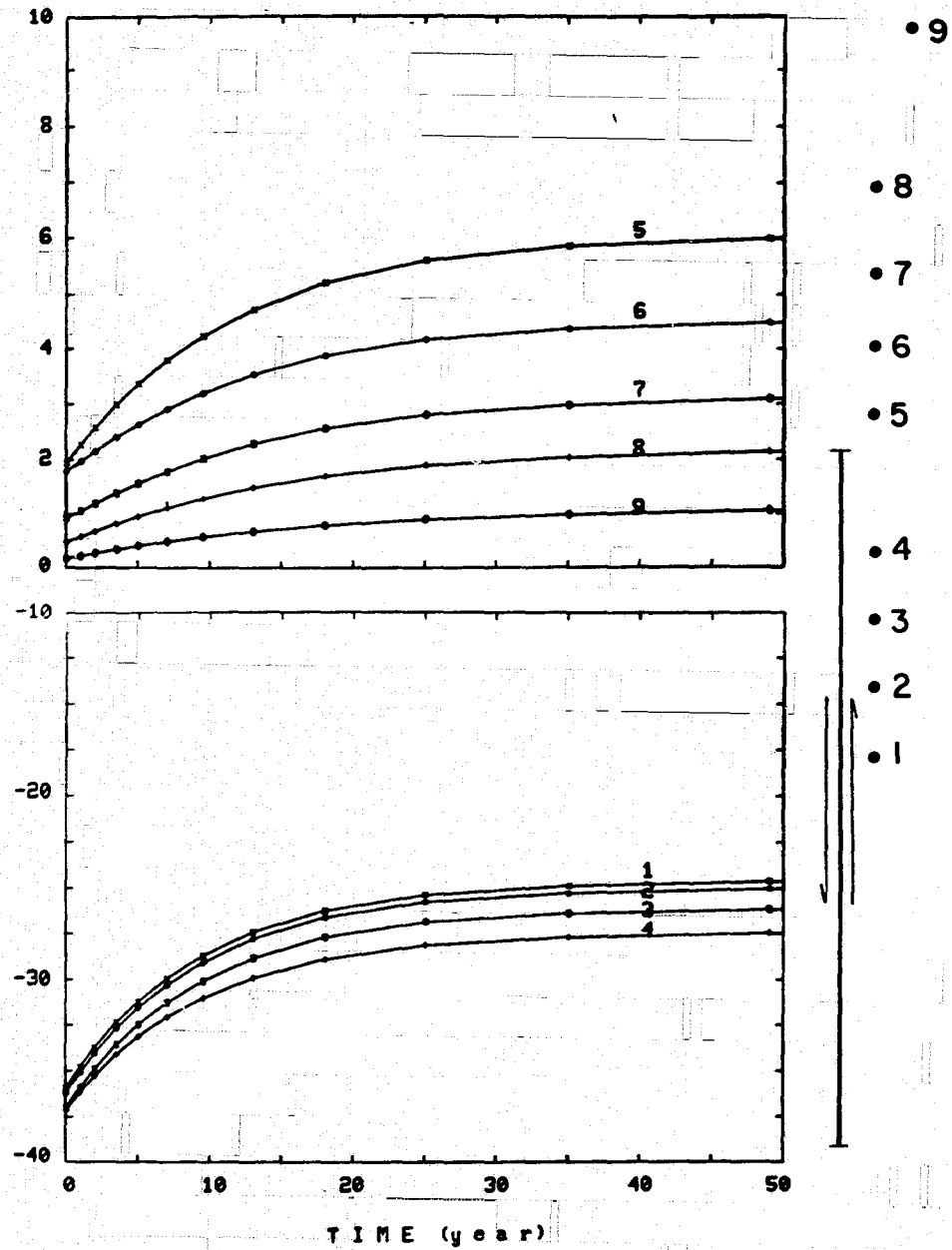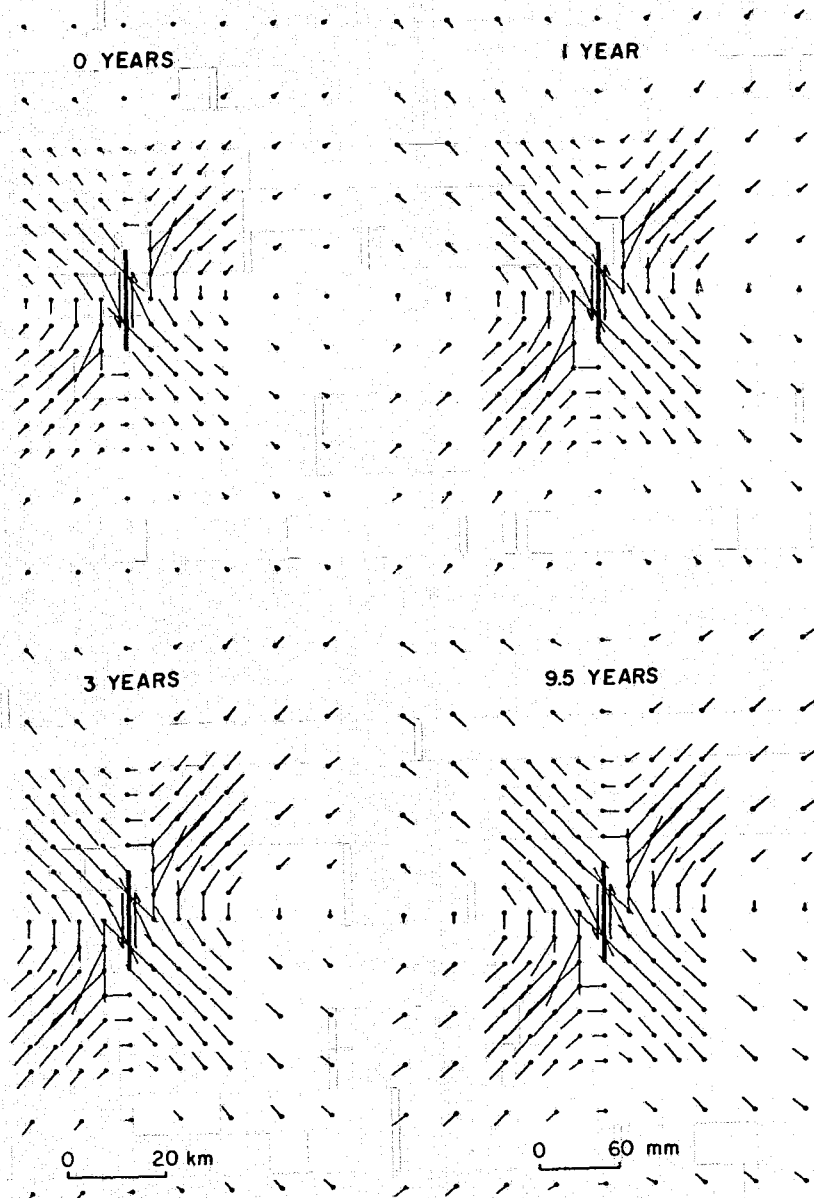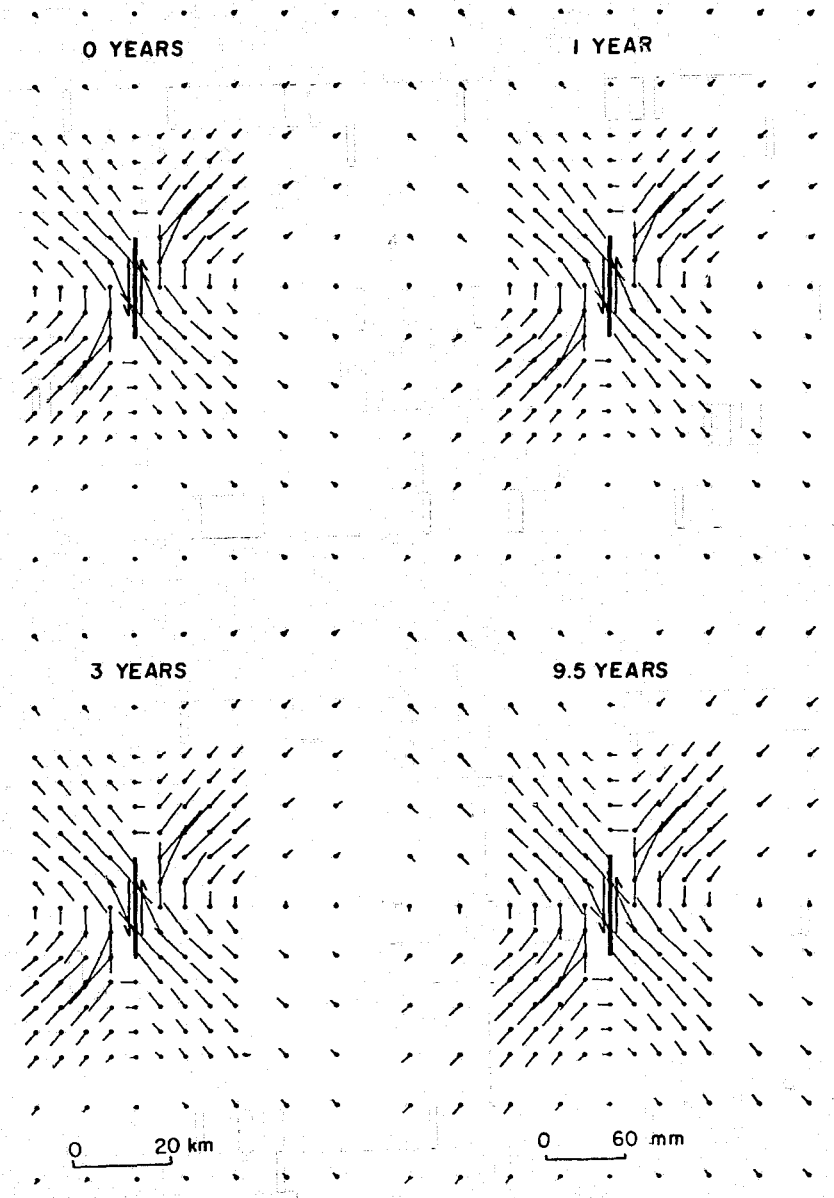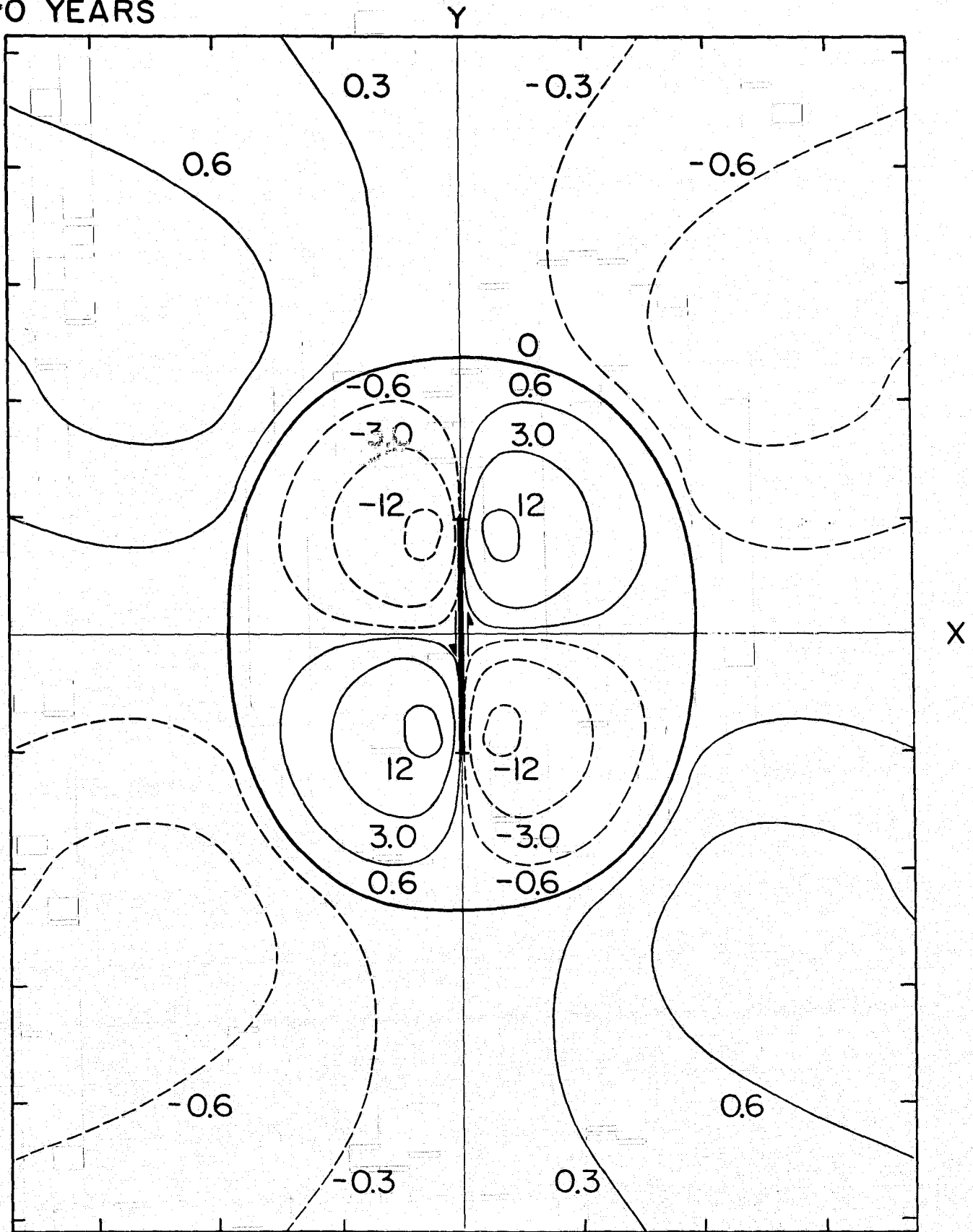
VERTICAL DISPLACEMENT
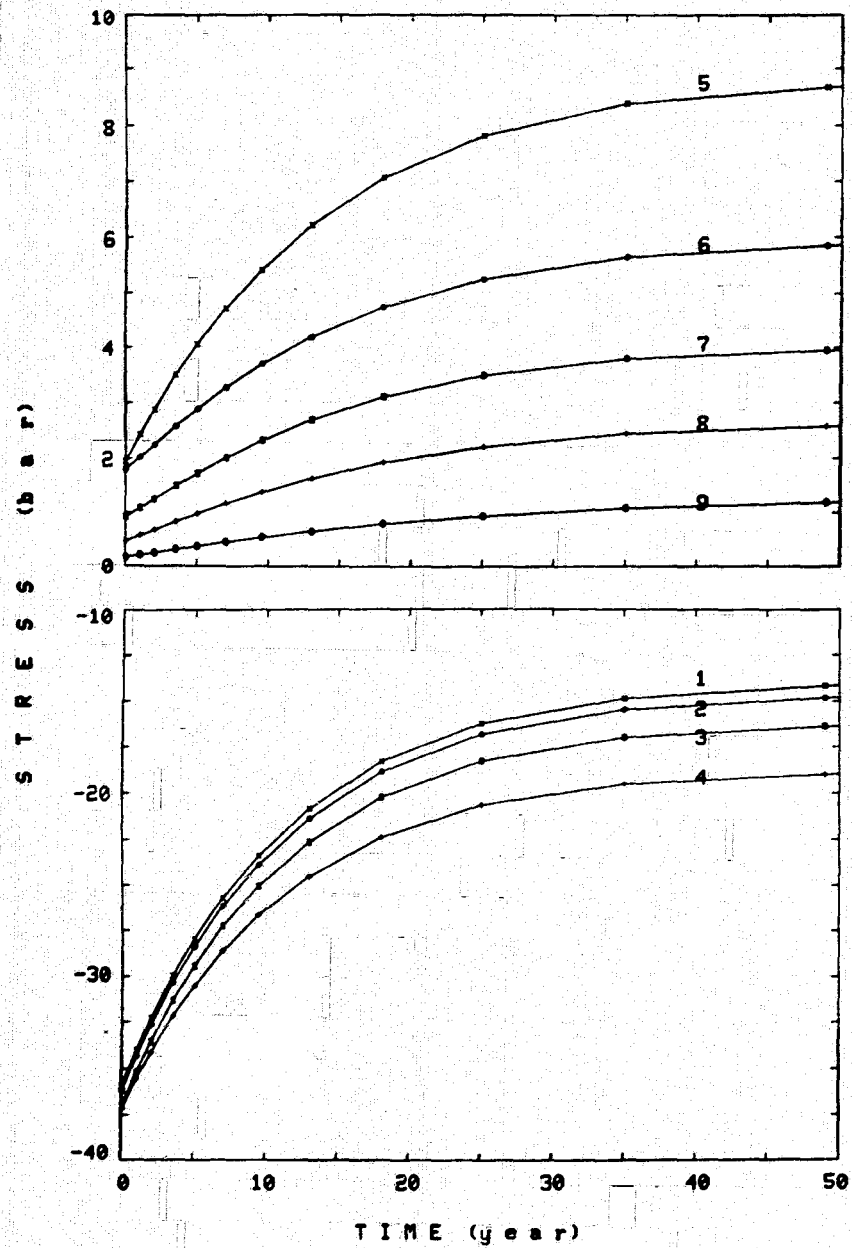
Fig. 16

(a)

9.5 YEARS

MODEL MI   VERT DISP CHANGE

(b)

9.5 YEARS
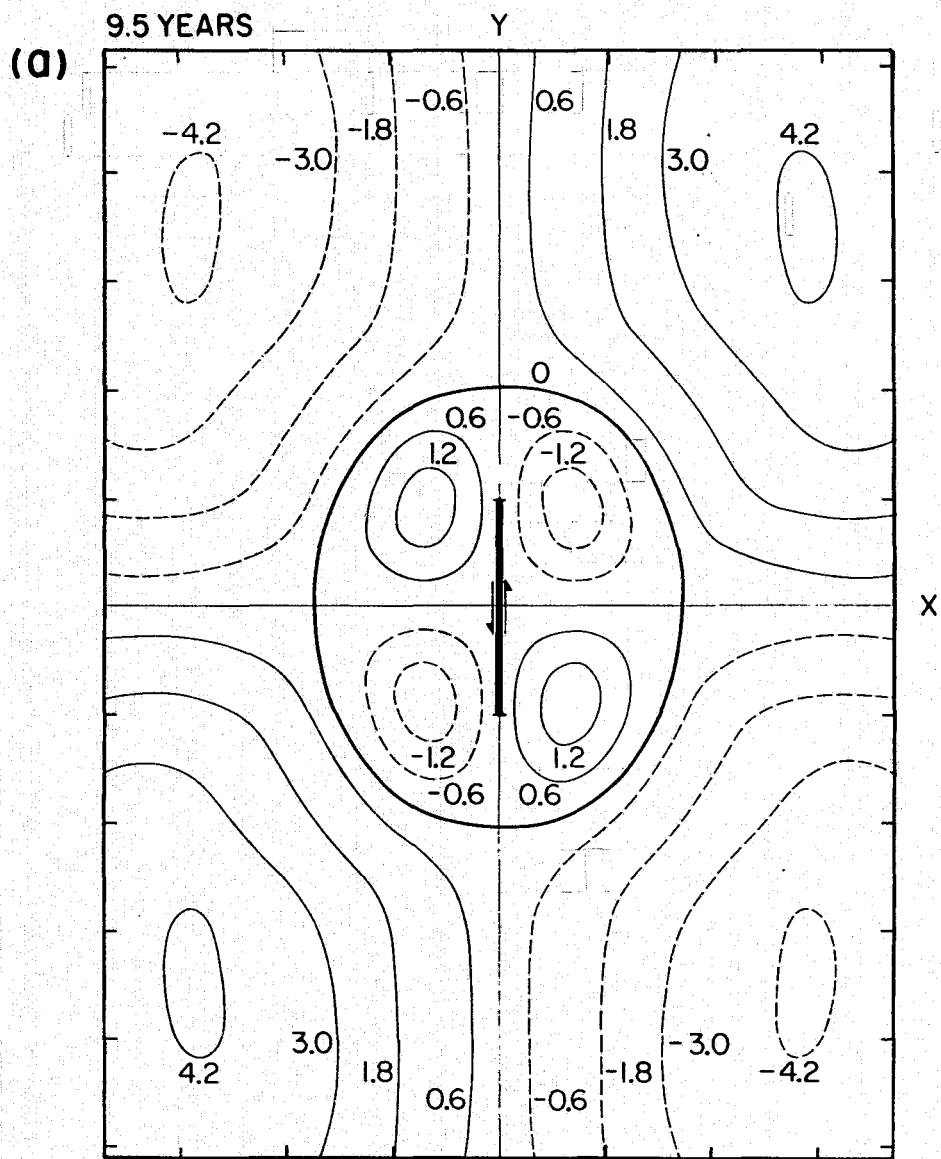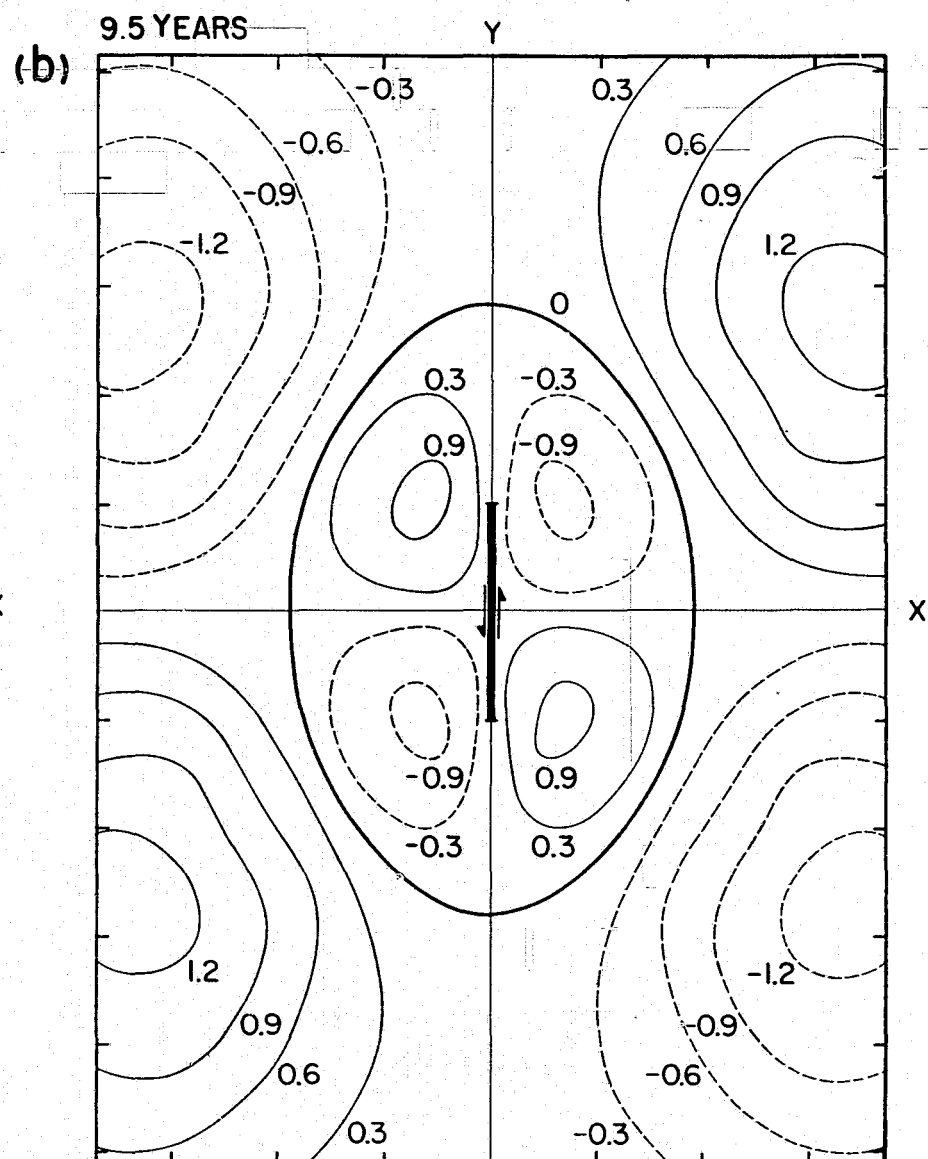
MODEL M2   VERT DISP CHANGE

Fig. 17
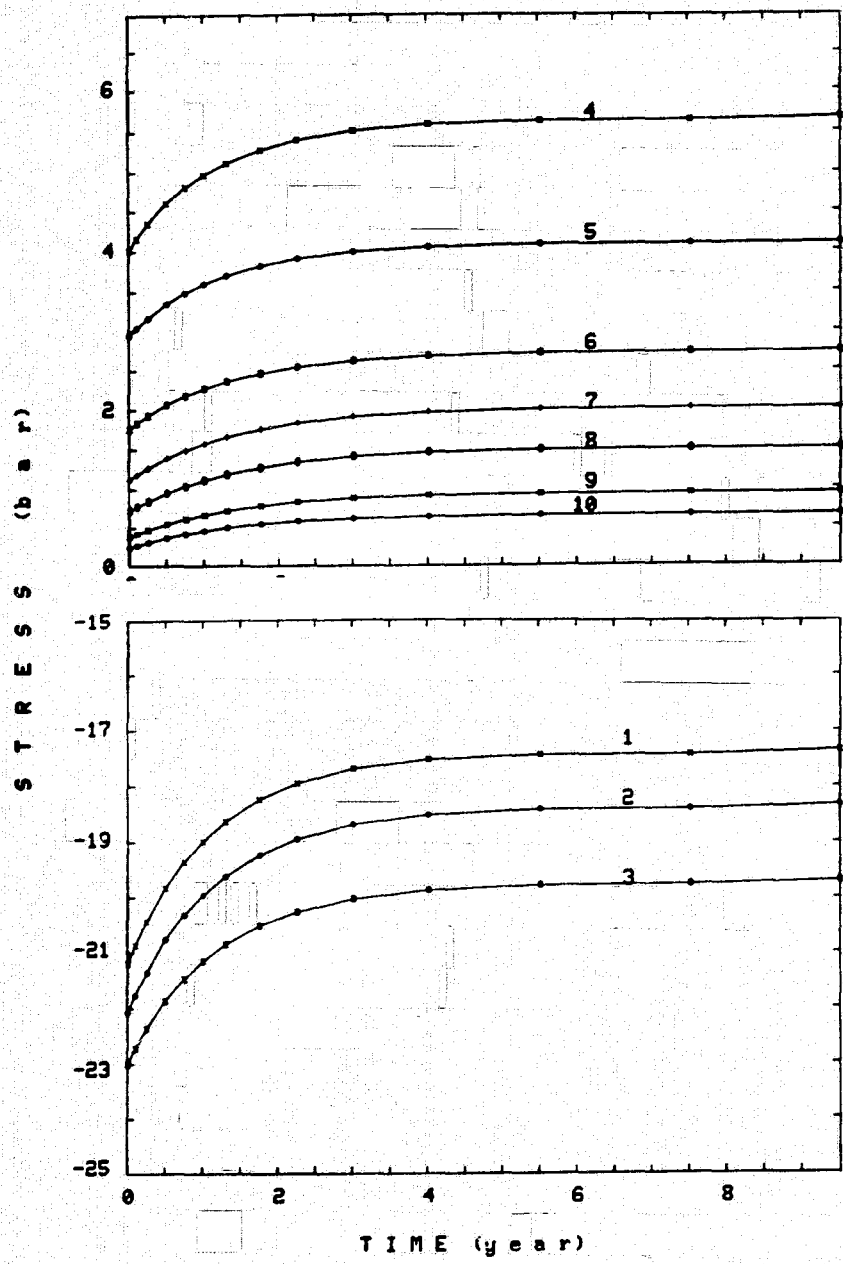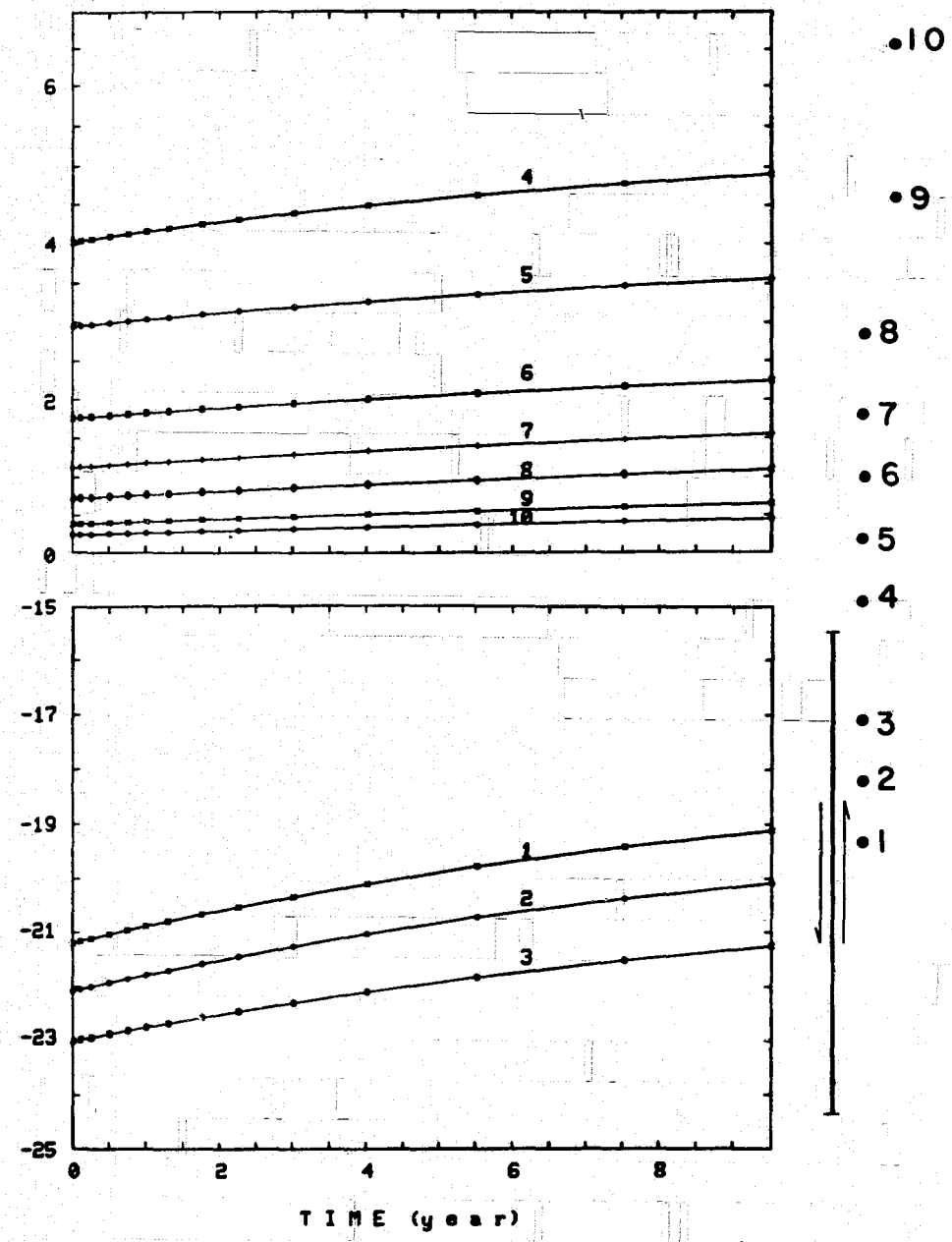
Fig. 18

PART 3: TECTONIC STRESS - MODELS AND MAGNITUDES

Introduction

Understanding the state of stress in the Earth's lithosphere is one of the paramount problems in Earth tectonics. The stress state is linked to causes - loading and unloading, heating and cooling, plate motions and driving forces, to consequences - creep deformation and seismic failure, and to rheology - the depth over which stress can be supported and the time dependence of material properties. None of the classes of links has been characterized in sufficiently quantitative detail to define the stress tensor in the lithosphere without ambiguity and without a long inference chain involving poorly tested assumptions. This paper deals with one cause of stress in the lithosphere: the system of forces that maintain plate motions. Specifically addressed are ways by which models of tectonic stress in the plates can be used to constrain the magnitude of regional deviatoric stress in the Earth's lithosphere.

Global models of the intraplate deviatoric stress that arises from the driving and resistive forces controlling plate motion have been given by Solomon et al. [1975] and Richardson et al. [1976, 1979]. A principal objective of those studies has been to find those sets of forces that best match the body of intraplate stress observations. The observations held to be most reliable for such comparisons are the indications of principal stress directions inferred from the mechanisms of

midplate earthquakes, from in situ stress measurements, and from the strikes of stress-sensitive geological features. While a comparison of model predictions and observations on the basis of principal stress orientations is straightforward and serves as a useful test by which to reject possible force models, such an exercise does not directly address the absolute magnitude of intraplate deviatoric stresses, since all deviatoric stresses in a model can be multiplied by an arbitrary constant without changing the relative magnitudes or the orientations of the principal stresses. We show in this paper, however, that under certain conditions the body of data on intraplate stress orientations does constrain the magnitude of tectonic stresses.

It might be argued that stress magnitudes can in principle be measured by direct in situ techniques in sufficient locations to characterize the stress field for length scales comparable to plate dimensions, thus obviating the need to apply indirect arguments to constrain tectonic stress magnitudes. This eventuality is doubtful for the near term, because of the difficulty of extrapolating near-surface measurements to greater depths in the lithosphere, and because further advances in technology will be necessary to conduct routinely measurements of in situ stress over the large fraction of the Earth's surface covered by oceans. On the basis of available hydrofracture data, it may at least be concluded that deviatoric stress magnitudes are on the order of several hundred bars to depths of several kilometers in a number of continental regions [Haimson, 1977; McGarr and Gay, 1978].

Thus the question remains: given the large and growing
body of data on the orientations of principal stresses within
the plates, what information on the magnitudes of regional
deviatoric stresses can be obtained from numerical models
for tectonic plate stresses? We discuss in this paper two
routes by which useful information on stress magnitudes can
be derived: (1) For the driving force models that best fit
the stress orientation data, if independent information on
the magnitude of one or more of the forces in the system can
be obtained, then the magnitudes of the total predicted
stress field are constrained to comparable precision. The
best fitting force models we have examined to date all involve
a significant contribution from ridge forces, the pushing
forces that arise because of the elevated topography of ridge
axes with respect to abyssal sea floor. Since ridges exert
forces equivalent to compressive plate stresses of 200-300
bars magnitude, this leads to the prediction that regional
deviatoric stresses are of this magnitude. (2) If in the
vicinity of a known local source of stress, the observations
of stress orientations indicate comparable control by the local
and regional stress field, then the magnitude of the regional
field may be estimated. This line of argument holds special
promise for oceanic intraplate regions where earthquakes
have occurred in the vicinity of islands or large bathymetric
features characterized by sufficiently good topographic and
gravity data to model the associated local lithospheric stress.

It should be mentioned that when direct in situ measurements of stress magnitudes have high reliability, the magnitude data can be used alongside the stress orientation data as a more powerful set of constraints on both regional and local forces on the lithosphere.

Stress Magnitudes and Global Plate Models

The comparison of predicted and observed directions of principal intraplate stresses can be a sensitive test of possible sources of stress. As noted above, if such a comparison indicates a significant contribution from a source of stress of known or estimable magnitude, then a strong constraint on the general magnitude of deviatoric stress in the lithosphere on regional scales is obtained. In this section, we summarize our recent work [Richardson et al., 1979] on testing global models of intraplate stress predicted by plate tectonic driving forces against observed directions of principal stresses, with particular emphasis on possible inferences on the magnitude of deviatoric stresses.

Premises. That observations of principal stress directions in the plates can be used to constrain plate tectonic driving force models requires the adoption of three working premises: (i) that regionally consistent stress orientation fields exist for large fractions of the stable interiors of plates, (ii) that such stress fields are steady over time periods less than that ($\sim 10^6$ years) characterizing changes in plate motions; and (iii) that a recognizable portion of these stress fields is dominated by contributions from plate tectonic forces.

The first premise has substantial observational support for most the plates [Sykes and Sbar, 1974; Sbar and Sykes, 1973; Richardson et al., 1979]; see Figure 1. The second premise depends on the question of whether in plate interiors the deformation and stress arising from past plate boundary slip superpose to produce steady motion and stress, or whether individual stress 'waves' from large earthquakes are discernible [e.g., Anderson, 1975]. This issue

may be resolved by ultra-precise geodetic measurements of short-term plate motions soon to be made [Niell et al., 1979; Smith et al., 1979; Bender et al., 1979 . The third premise will be the most difficult to establish with certainty, but is a reasonable working hpyothesis for regions well removed from such other notable sources of stress as recent tectonic or thermal activity, recent topographic loading or unloading, and pronounced structural heterogeneities.

Possible Driving Forces. We consider several simply parame-terized driving and resistive forces as potential elements of a plate tectonic force model: plate boundary forces at ridges, trenches, transform faults and zones of continent-continent collision; and basal forces associated with viscous interaction between the lithosphere and the asthenosphere. While all of these forces contribute to lithospheric stress, it is important to recognize that potentially large stress contributions can also arise from lithospheric cooling [Turcotte and Oxburgh, 1973] , latitudinal plate motion [Turcotte and Oxburgh, 1973] , crustal thickness inhomogeneities [Artyushkov, 1973] , lithospheric loading and unloading [Walcott, 1970; Watts and Cochran, 1974; Haxby and Turcotte, 1976] and past tectonic events [Swolfs et al., 1974; Tullis, 1977] . In the interpretation of stress observations in terms of plate driving forces, care must be exercised to remove or to avoid where possible the effects of these additional sources of lithospheric stress.

The compressive stress produced in oceanic plates by the elevation of mid-ocean ridges is the easiest to quantify among the set of possible driving and resistive forces, and is in the

range 200-300 bars [Hales, 1969; Frank, 1972; McKenzie, 1972].

At subduction zones, the negative buoyancy of subducted litho-

sphere is capable of exerting an extensional force equivalent to **several**

kilobars stress on the adjacent plates [McKenzie, 1969; Turcotte

and Schubert, 1971], but the greater fraction of available

pulling force is counterbalanced by forces resisting descent of

the slab into the mantle [Smith and Toksöz, 1972; Forsyth and

Uyeda, 1975; Richter, 1977]. The net pull by slabs on the

surface plates is uncertain but is considerably smaller than that

due to available negative buoyancy. At zones of continent-

continent collision, the net force on the adjacent plates may be

resistive (net compression), because of the contribution from the

excess topography of the mountain belt marking the collision

zone; the contribution from topography involves shear stresses

of 200-300 bars for the main boundary fault at the base of the

Himalayas [Bird, 1978]. The resistive force at

transform faults is uncertain [Brune et al.,

1969; Brace and Byerlee, 1970], but is not likely to be a major

contributor to the plate driving mechanism on the basis of the

relatively small fraction of boundary taken up by transforms for

most plates and the poor correlation of plate speeds with length

of transform boundary [Forsyth and Uyeda, 1975; Aggarwal, 1978].

The viscous traction at the base of the plates is less well

characterized than plate boundary forces and is uncertain both in

magnitude and in direction. The uncertainties are linked to

questions of the radial scale for upper mantle convection, the

planform for 'counterflow' to balance plate creation and destruc-

tion, and the existence of a smaller secondary scale of astheno-

spheric convection to transport heat [Richter and Parsons, 1975;

McKenzie and Weiss, 1975; Harper, 1978; Chase, 1979; Hager and O'Connell, 1979]. Some simple forms for viscous drag are adopted as a basis for testing models, but the various potential complexities must be kept in mind.

Stress Models. A variety of driving force models incorporating different relative amounts of boundary forces and basal tractions as described above have been tested against the observations of intraplate stress orientations. The lithosphere is modeled as a thin, spherical, elastic shell, and stresses are calculated from the imposed forces using the finite-element analysis described by Richardson [1978]. The results of many models are given in Richardson et al. [1979], and only a summary of the results pertinent to the question of stress magnitudes will be given here.

A summary of stress orientation data for intraplate regions is given in Figure 1. Most of the data come from the mechanisms of intraplate earthquakes; the re-mainder are from in situ measurements (see Richardson et al. [1979] for the original sources of the data shown). In compiling such a data set, it is necessary to establish criteria for the selection of those data most appropriate for constraining the tectonic stress field. While such criteria are of necessity at least partly arbitrary, our approach has been to exclude only those data very near ($\sim$100 km distance or less) plate boundaries and those data likely reflecting unmodeled processes. Thus data from continental margins

have been excluded on the basis of possible contributions from sediment loading or thermal contraction - effects not modeled, and data are not used from regions of complex tectonics not likely to be a response solely to plate-scale forces (e.g., Alps, Appalachians, and North America west of the Rockies).

Based on a comparison with the observed stress orientations in Figure 1, the predicted stresses are in best agreement with the observations when pushing forces at ridges are included in the driving force model and when the net pulling force due to subducted lithosphere is comparable in magnitude or is at most a few times larger than other forces acting on the plates. On the basis of intraplate stresses, therefore, resistive forces opposing the motion of the slab with respect to the mantle must nearly balance the negative buoyancy of the relatively cool, dense slab, in agreement with similar conclusions derived from other considerations [Smith and Toksöz, 1972; Forsyth and Uyeda, 1975, Richter, 1977]. The maximum ratio of net slab pull to net ridge push is not sensitive to a dependence of net slab pull on subduction rate or to the inclusion of other forces in the system. Forces

resisting further convergence at continental collision zones
along the Eurasian plate are important for intraplate stresses,
and improve the fit to the data in Europe, Asia, and the Indian
plate. Resistive viscous drag forces acting on the base of the
plate in a direction opposite to "absolute" plate velocity
improve the fit to the intraplate stress field for several plates
(e.g., Nazca, South America). The intraplate stress field is relatively
insensitive to an increased drag coefficient beneath old
oceanic lithosphere compared to young oceanic or continental
lithosphere. Increasing by a factor of five or ten the drag
coefficient beneath continental relative to oceanic lithosphere
changes the calculated stresses only slightly and has little
effect on the overall fit to observed stresses as long as some
resistive drag acts beneath oceanic plates.

Models in which drag forces drive (i.e., act parallel to
"absolute" plate velocity) rather than resist plate motions are
in poor agreement with the data. This poor agreement may depend
on the oversimplified model of the adopted interaction between
the plate and the asthenosphere. As noted above, the actual flow
pattern in the mantle, including counterflow and possible multiple
scales of convection, may be considerably more complicated than has
been assumed in these models.

Two models that provide reasonably good fits to a large
fraction of the intraplate stress orientation data are shown in
Figures 2 and 3. In Figure 2 are shown the predicted intraplate
stresses for a model with the following forces: (i) a symmetric
pushing force at ridges equivalent to a compressive stress of 100
bars across a 100 km thick plate, (ii) a symmetric pulling force

at trenches of the same absolute magnitude, (iii) a symmetric
resistive force at continental collision zones of the same
absolute magnitude and (iv) a drag stress $-D\underline{v}$, where $\underline{v}$ is absolute
plate velocity in cm/yr and D is 0.1 bar/cm/yr beneath oceans and
0.6 bar/cm/yr beneath continents. Note that only the relative
magnitudes of these forces are constrained by the stress orienta-
tion data; their absolute magnitudes are proportional to an un-
specified multiplicative constant.

The predicted directions of principal stresses for this force
model are in good agreement with the data for eastern North
America, Europe, Asia near the Himalayas, and the Indian plate.
The fit to the data is good in South America, especially far from
the trench, and in western Africa and is acceptable in most of the
Pacific plate. The orientation of the calculated maximum compres-
sive stress in the Nazca plate for the model is only in moderate
agreement with the orientation inferred from the single fault
plane solution available. The fit to the data in the northern
Pacific, eastern Asia, and east Africa is rather poor. The fit
to the data in the northern Pacific and eastern Asia could
be improved if subduction zone or drag forces were decreased along
the western Pacific plate margin or if slab forces were concentrated
on the subducted plate. No attempt, however, has been made to vary
plate boundary forces locally to match inferred stresses. If such
an approach were adopted, most observed stresses could
be matched but the solution for the driving mechanism would be
unjustifiably arbitrary and non-unique.

In Figure 3 are shown the intraplate stresses for a force
model that takes the approach of Davies [1978] and Richardson

[1978] based on the assumption that drag balances the net torque
on each plate due to boundary forces. The resulting drag thus
varies from plate to plate and need not bear a simple relation-
ship to relative plate motions, in contrast to the drag derived
from absolute plate motion models consistent with known relative
velocities [Solomon and Sleep, 1974; Solomon et al., 1975;
Minster et al., 1974]. The force model includes: (i) a symmetric
force at ridges equivalent to a compressive stress of 100 bars
across a 100-km thick plate, (ii) a symmetric resistive force at conti-
nental convergence zones of twice this magnitude, (iii) a pulling force
at trenches, on the subducted plate only, equivalent to an exten-
sional stress of 100 bars across a 100-km thick plate, and (v) a
viscous drag on each plate, due to the rotation of the plate with
respect to the underlying mantle (which may be moving), determined
by balancing the total vector torque on the plate from boundary forces.

The predicted stress directions for this model (Figure 3)
agree very well with the data for several areas. In the North
American and Nazca plates, the orientation of the maximum compres-
sive stress is well matched by the model. The fit is almost as
good   in Europe and in Asia north of the Himalayas. In the Indian
plate, compressive stresses trend NW-SE in continental India, in
agreement with the data, but the fit is poorer in Australia. In
South America, the maximum compressive stress trends E-W, in only
moderate agreement with the data. In the Pacific and the eastern
part of the African plate the agreement with the data is poor. On
the whole, this model provides a better fit to continental than
oceanic data. Comparison of Figures 2 and 3 suggests that any force
pulling the overthrust plate toward the trench is probably lower in

magnitude than the net pull on the subducted plate.

Discussion. From the standpoint of deviatoric stress magnitudes, the most important general conclusion from the modeling of plate tectonic stresses and the comparison with intraplate stress orientation data is that ridge pushing forces are an important element of the set of driving forces for the models that provide the best fit to observations. The stresses that arise from ridge topography are 200-300 bars compression, as noted above. We are thus led to the conclusion that regional deviatoric stresses in plate interiors are of this same general magnitude, or 200-300 bars to within a factor of perhaps 2 to 3.

This conclusion should be tempered, however, by several general observations on the results of the plate tectonic stress models. The models represented in Figures 2 and 3, though providing good matches to the data for a number of regions with well characterized stresses, do not fit all of the data. Thus either there are simple models not tested that provide a better fit to the global data set than those shown, or the stress observations are influenced by processes not included in the simple models. Even if a model were obtained that fit all reliable observations to within their estimated errors, it is likely on the basis of models tested to date that this model would not be unique. Thus statements based on elements of best-fitting force models must be understood in recognition of this nonuniqueness.

Stress Magnitudes and Local vs. Regional Stresses

An alternative approach to constrain the magnitude of regional deviatoric stresses in the lithosphere from stress orientation data and plate tectonic models is to find situations in which observed stress orientations are sensitive in approximately equal measure to a local stress field that may be readily quantified and to a regional stress field whose magnitude is to be determined. Such an approach holds high promise for constraining the magnitudes of plate tectonic stresses in oceanic lithosphere.

Consider the effect of a volcanic load on oceanic lithosphere. Such a load leads to lithospheric flexure and to potentially large local bending stresses. For a very large load, such as Hawaii, the local stresses may be in excess of 1 kbar [Walcott, 1970; Watts and Cochran, 1974] and may dominate the regional stress. That bending stresses may dominate regional stresses for Hawaii is supported by the report by Rogers and Endo [1977] that greatest compressive stress axes from composite fault plane solutions for many mantle earthquakes beneath and near the island of Hawaii are radial with respect to the island.

For loads appropriately smaller in magnitude than Hawaii, the local stresses should be comparable in magnitude to the regional stresses. Thus the mechanisms of earthquakes in the vicinity of such loads might be expected to indicate P and T axes which differ somewhat from regional trends but which are not predictable simply from stress models for the local load only. For earthquakes near very small loads or distant from any pronounced topographic relief, the mechanisms should reflect the regional

stress field.

As an illustration of this approach, consider the region
near the Ninetyeast ridge in the central Indian Ocean. The
Ninetyeast ridge is a pronounced linear feature some 5000 km
long and rising 1500-2000 m above the surrounding seafloor
[e.g., Bowin, 1973]. The ridge is isostatically compensated
except at short wavelengths [Bowin, 1973; Detrick and Watts,
1979]. Several large earthquakes have occurred in the Indian
plate in the general vicinity during this century [Sykes,
1970; Stein and Okal, 1978].

The orientation of principal stresses in the Indian plate
may be estimated from the fault plane solutions of intraplate
earthquakes. Figure 4 shows the P axis orientations for all large
earthquakes with known focal mechanisms in the Indian plate near the
Ninetyeast ridge. There is a strongly regionally consistent
NW-SE trend to the direction of inferred greatest compressive
stress.

Two aspects of this general consistency are noteworthy:
(i) The P axes for strike-slip events on and near the Ninetyeast
ridge trend in general agreement with those for thrust events
in the plate off the ridge. Thus while a zone of weakness
associated with the ridge may control the type of faulting
[Stein and Okal, 1978], the inferred direction of maximum
horizontal stress for Ninetyeast ridge events is still
reliable. The data in Figure 4 are entirely consistent
with a generally uniform stress field across the portion of

the Indian plate shown, with strike-slip rather than thrust motion the preferred fault type within weak zones in the lithosphere.   (ii) The P axes for thrust events off the Ninetyeast ridge are not orthogonal to the strike of the ridge.   Thus stresses associated with ridge topography do not dominate the local stress field.

This second conclusion can be quantified to produce a constraint on the magnitude of the regional stress field. Adopting Bowin's [1973] model for the isostatic compensation of the Ninetyeast ridge, the compressive force that the ridge exerts per unit length on the lithosphere beneath the adjacent abyssal plain may be estimated from equations (47-49) in Artyushkov [1973]:

$$\Sigma = \int (\sigma_{xx} - \sigma_{zz}) dz$$
$$= - (.14\zeta + .067\zeta^2) \times 10^9 \text{ bar-cm} + \Sigma_{ridge} \qquad (1)$$

where σ_{xx} and σ_{zz} are horizontal and vertical normal stress components ($\sim$ principal stresses), ζ is the height of the ridge (in km) with respect to the abyssal plain, Σ_{ridge} is the value of Σ beneath the ridge, the integral is taken over the depth range of horizontal density variations, and the minus sign denotes a compressive force. Note that (1) includes the effects of topography and isostatic compensation only; the effects of viscous forces at the base of the plate and of thermal stress due to any differential cooling between the ridge and surrounding sea floor, for instance, are not included. For ζ = 1.5 to 2 km [Bowin, 1973], (1) gives $\Sigma - \Sigma_{ridge}$ =

- (0.35 to 0.54) x 10^9 bar-cm, or the equivalent of 70

to 110 bars additional horizontal deviatoric stress over a

50 km thick plate. For comparison, <u>Artyushkov</u> [1973] gives

- 1.2 x 10^9 bar-cm and 240 bars compression for the force/

length and stress associated with spreading ridges.

Thus the regional deviatoric stresses in the Indian plate
(excluding the contribution from the Ninetyeast ridge) must
be larger than ~100 bar in magnitude in order to account for
the pattern of stress orientations in Figure 4. This result
provides only a lower bound on the magnitude of regional
deviatoric stresses in one plate, but the result
is at least consistent with the inference made above that
regional stresses are similar in magnitude to the stresses
produced by ridge forces, which are 3 ± 1 times as large as
the force exerted by Ninetyeast ridge topography.

A number of other oceanic intraplate earthquakes large
enough so that their focal mechanisms are known have occurred
in close proximity to prominent bathymetric features.

Bergman and Solomon [1980] have compiled a comprehensive catalog of 159 oceanic intraplate earthquakes and, for a representative subset of 83 epicentral regions, have assessed the degree of association of these earthquakes with large bathymetric features and with zones of expected lithospheric weakness (e.g., fracture zones). A histogram of the results (Figure 5) shows that the epicenters of at least 12 oceanic intraplate earthquakes with known focal mechanisms, and at least 11 additional earthquake localities with one or more $m_b \geq 4.7$ events since 1964, are situated near features of pronounced seafloor topography. Several of these features involve lithospheric loads that should lead to bending stresses larger than the stresses indicated above for the Ninetyeast ridge. Thus it may be possible by a combination of detailed stress models and careful source mechanisms to bound regional deviatoric stress magnitudes from both above and below using this approach.

Two potential difficulties with this approach should, however, be noted: (i) Many oceanic intraplate earthquakes occur in or near such obvious zones of weakness as fracture zones and volcanic areas. Over 70 percent of the oceanic earthquake epicentral regions in the listing of Bergman and Solomon [1980] are located in such areas (Figure 5).Stress directions

inferred from earthquake mechanisms for such events should be used only with caution in the absence of corroborative information from events removed from the weak zone (e.g., Figure 4). (ii) Bending stresses associated with lithospheric flexure, for given rheology and thermal structure, are extremely sensitive to depth. Thus for an observation of stress orientation from an earthquake mechanism to be a useful constraint on stress amplitude, the focal depth must be known with high precision, probably to within a few kilometers.

Conclusions

The global data on directions of principal stresses in plate interiors can serve as a test of possible plate tectonic force models. Such tests conducted to date favor force models in which ridge pushing forces play a significant role. For such models, the general magnitude of regional deviatoric stresses is comparable to the 200-300 bars compressive stress exerted by spreading ridges.

An alternative approach to estimating magnitudes of regional deviatoric stresses from stress orientations is to look for regions of local stress either demonstrably smaller than or larger than the regional stresses. The regional stresses in oceanic intraplate regions are larger than the ~ 100 bar compression exerted by the Ninetyeast ridge and less than the bending stresses (≥ 1 kbar) beneath Hawaii.

C-2

Acknowledgements

RERENCES

Aggarwal, Y.P., Scaling laws for global plate motions: conse-
quences for the driving mechanism, interplate stresses and
mantle viscosity (abstract), Eos Trans. Amer. Geophys. Un.,
59, 1202, 1978.

Anderson, D.L., Accelerated plate tectonics, Science, 187, 1077-
1079, 1975.

Artyushkov, E.V., Stresses in the lithosphere caused by crustal
thickness inhomogeneities, J. Geophys. Res., 78, 7675-7708,
1973.

Bender, P.L., J.E. Faller, J. Levine, S. Moody, M.R. Pearlman,
and E.C. Silverberg, Possible high-mobility LAGEOS ranging
station, Tectonophysics, 52, 69-73, 1979.

Bergman, E.A., and S.C. Solomon, Oceanic intraplate earthquakes:
implications for local and regional intraplate stress, J.
Geophys. Res., submitted, 1980.

Bird, P., Initiation of intracontinental subduction in the
Himalaya, J. Geophys. Res., 83, 4975-4987, 1978.

Bowin, C., Origin of the Ninety East ridge from studies near the
equator, J. Geophys. Res., 78, 6029-6043, 1973.

Brace, W.F., and J. D. Byerlee, California earthquakes: why
only shallow focus?, Science, 168, 1573-1575, 1970.

Brune, J.N., T.L. Henyey, and R.F. Roy, Heat flow, stress, and
rate of slip along the San Andreas fault, California, J.
Geophys. Res., 74, 3821-3827, 1969.

Chase, C.G., Asthenospheric counterflow: a kinematic model,
Geophys. J. Roy. Astron. Soc., 56, 1-18, 1979.

Davies, G.F., The roles of boundary friction, basal shear
stress and deep mantle convection in plate tectonics,
Geophys. Res. Lett., 5, 161-164, 1978.

Detrick, R.S., and A.B. Watts, An analysis of isostasy in the world's oceans, 3, aseismic ridges, J. Geophys. Res., 3637-3653, 1979.

Fitch, T.J., Plate convergence, transcurrent faults, and internal deformation adjacent to southeast Asia and the western Pacific, J. Geophys. Res., 77, 4432-4460, 1972.

Forsyth, D.W., and S. Uyeda, On the relative importance of driving forces of plate motion, Geophys. J. Roy. Astron. Soc., 43, 163-200, 1975.

Frank, F.C., Plate tectonics, the analogy with glacier flow and isostasy, in Flow and Fracture of Rocks, Am. Geophys. Un., Geophys. Mon. 16, 285-292, 1972.

Hager, B.H., and R.J. O'Connell, Kinematic models of large-scale flow in the earth's mantle, J. Geophys. Res., 84, 1031-1048, 1979.

Haimson, B.C., Crustal stress in the continental United States as derived from hydrofracturing tests, in The Earth's Crust, Geophys. Monogr. 20, J.C. Heacock, ed., AGU, Washington, D.C., 576-592, 1977.

Hales, A.L., Gravitational sliding and continental drift, Earth Planet. Sci. Lett., 6, 31-34, 1969.

Harper, J.F., Asthenosphere flow and plate motions, Geophys. J. Roy. Astron. Soc., 55, 87-110, 1978.

Haxby, W.F., and D.L. Turcotte, Stresses induced by the addition or removal of overburden and associated thermal effects, Geology, 4, 181-184, 1976.

McGarr, A., and N.C. Gay, State of stress in the earth's crust, Ann. Rev. Earth Planet. Sci., 6, 405-436, 1978.

McKenzie, D.P., Speculations on the consequences and causes of plate motions, Geophys. J. Roy. Astron. Soc., 18, 1-32, 1969.

McKenzie, D.P., Plate tectonics, in The Nature of the Solid Earth, ed. E.C. Robertson, McGraw-Hill, New York, 323-360, 1972.

McKenzie, D.P., and N.O. Weiss, Speculations on the thermal and tectonic history of the earth, Geophys. J. Roy. Astron. Soc., 42, 131-174, 1975.

Minster, J.B., T.H. Jordan, P. Molnar, and E. Haines, Numerical modeling of instaneous plate tectonics, Geophys. J. Roy. Astron. Soc., 36, 541-576, 1974.

Neill, A.E., K.M. Ong , P.F. MacDoran, G.M. Resch, D.D. Morabito, E.S. Claflin, and J.F. Dracup, Comparison of a radio interferometric differential baseline measurement with conventional geodesy, Tectonophysics, 52, 49-58, 1979.

Richardson, R.M., Finite element modeling of stress in the Nazca plate: driving forces and plate boundary earthquakes, Tectonophysics, 50, 223-248, 1978.

Richardson, R.M., S.C. Solomon, and N.H. Sleep, Intraplate stress as an indicator of plate tectonic driving forces, J. Geophys. Res., 81, 1847-1856, 1976.

Richardson, R. M., S.C. Solomon and N.H. Sleep, Tectonic stress in the plates, Rev. Geophys. Space Phys., 17, 981-1019, 1979.

Richter, F.M., On the driving mechanism of plate tectonics, Tectonophysics, 38, 61-88, 1977.

Richter, F.M. and B. Parsons, On the interaction of two scales of convection in the mantle, J. Geophys. Res., 80, 2529-2541, 1975.

Rogers, D.B. and E.T. Endo, Focal mechanisms for upper mantle earthquakes and flexure of the lithosphere near Hawaii (abstract), Eos Trans. Amer. Geophys. Un., 58, 1231, 1977.

Sbar, M.L., and L.R. Sykes, Contemporary compressive stress and seismicity in eastern North America: an example of intraplate tectonics, Geol. Soc. Am. Bull., 84, 1861-1882, 1973.

Smith, A.T., and M.N. Toksöz, Stress distribution beneath island

arcs, Geophys. J. Roy. Astron. Soc., 29, 289-318, 1972.

Smith, D.E., R. Kolenkiewicz, P.J. Dunn and M.H. Torrence, The
measurement of fault motion by satellite laser ranging,
Tectonophysics, 52, 59-67, 1979.

Solomon, S.C., and N.H. Sleep, Some simple physical models for
absolute plate motions, J. Geophys. Res., 79, 2557-2567,
1974.

Solomon, S.C., H.H. Sleep, and R. M. Richardson, On the forces
driving plate tectonics: inferences from absolute plate
velocities and intraplate stress, Geophys. J. Roy. Astron.
Soc., 42, 769-801, 1975.

Stein, S., and E.A. Okal, Seismicity and tectonics of the Ninety-
east ridge area: evidence for internal deformation of the
Indian plate, J. Geophys. Res., 83, 2233-2245, 1978.

Sykes, L.R., Seismicity of the Indian Ocean and a possible nascent
island arc between Ceylon and Australia, J. Geophys. Res.,
75, 5041-5055, 1970.

Sykes, L.R., and M.L. Sbar, Focal mechanism solutions of intra-
plate earthquakes and stresses in the lithosphere, in Geo-
dynamics of Iceland and the North Atlantic Area., ed. by L.
Kristjansson, D. Reidel, Dordrecht, Holland, 207-224, 1974.

Swolfs, H.S., Jr., J. Handin, and H.R. Pratt, Field measurements
of residual strain in granitic rock masses, in Advances in
Rock Mechanics, Proceedings of the 3rd Congress, Interna-
tional Society for Rock Mechanics, Vol. 2A, National Academy
of Sciences, Washington, DC, pp. 563-568, 1974.

Tullis, T.E., Reflections on measurement of residual stress in
rock, Pure Appl. Geophys., 115, 57-68, 1977.

Turcotte, D.L., and E.R. Oxburgh, Mid-plate tectonics, *Nature*, *244*, 337-339, 1973.

Turcotte, D.L. and G. Schubert, Structure of the olivine-spinel phase boundary in the descending lithosphere, *J. Geophys. Res.*, *76*, 7980-7987, 1971.

Walcott, R.I., Flexure of the lithosphere at Hawaii, *Tectono-physics*, *9*, 435-446, 1970.

Watts, A.B. and J.R. Cochran, Gravity anomalies and flexure of the lithosphere along the Hawaiian-Emperor seamount chain, *Geophys. J. Roy. Astron. Soc.*, *38*, 119-141, 1974.

Figure Captions

Figure 1. A summary of intraplate stress orientation data
[Richardson et al., 1979]. Filled circles denote fault
plane solutions; arrows denote P and T axes, where nearly
horizontal.   Filled circles without arrows denote thrust
faults with poorly constrained P axes. Open circles
represent in situ data; the line gives the direction of
maximum horizontal compressive stress.

Figure 2. Principal horizontal deviatoric stresses in the
lithosphere for a model of plate driving forces (see text).
Principal stress axes without arrows and with arrows pointing
outward denote deviatoric compression and tension, respec-
tively. Relative magnitude of principal stresses is indicated
by the length of stress axes. From Richardson et al. [1979].

Figure 3. Principal horizontal deviatoric stresses in the litho-
sphere for an alternative driving force model in which basal
shear balances the torque due to boundary forces for each
plate (see text). From Richardson et al. [1979].

Figure 4. Summary of focal mechanisms for earthquakes in the Ninety-
east ridge region of the Indian plate. Fault plane solutions
are shown as equal area projections; compressional quadrants
are shaded. Lines through each solution denote the orienta-
tion of the P axis. Data are from Sykes [1970], Fitch [1972],
Sykes and Sbar [1974], Stein and Okal [1978], and Bergman and
Solomon [1980].

Figure 5. Histograms of the number of oceanic intraplate earthquake

   epicentral regions in the catalog of Bergman and Solomon

   [1980] sorted by likelihood of association with either (left)

   pre-existing zones of weakness, such as fracture zones or

   volcanic seamount chains, or (right) with topographic relief

   that may provide a significant local source of stress.
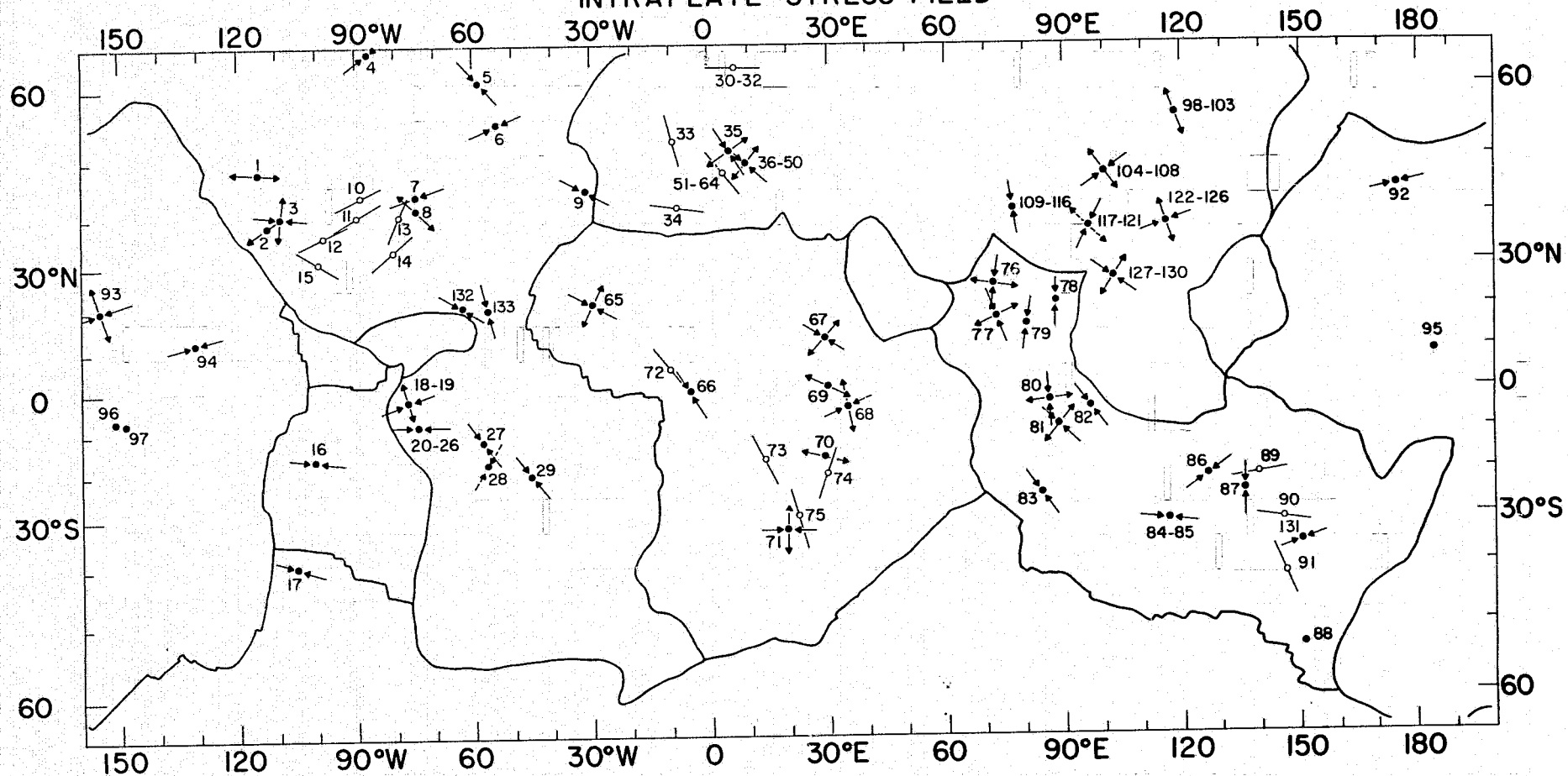
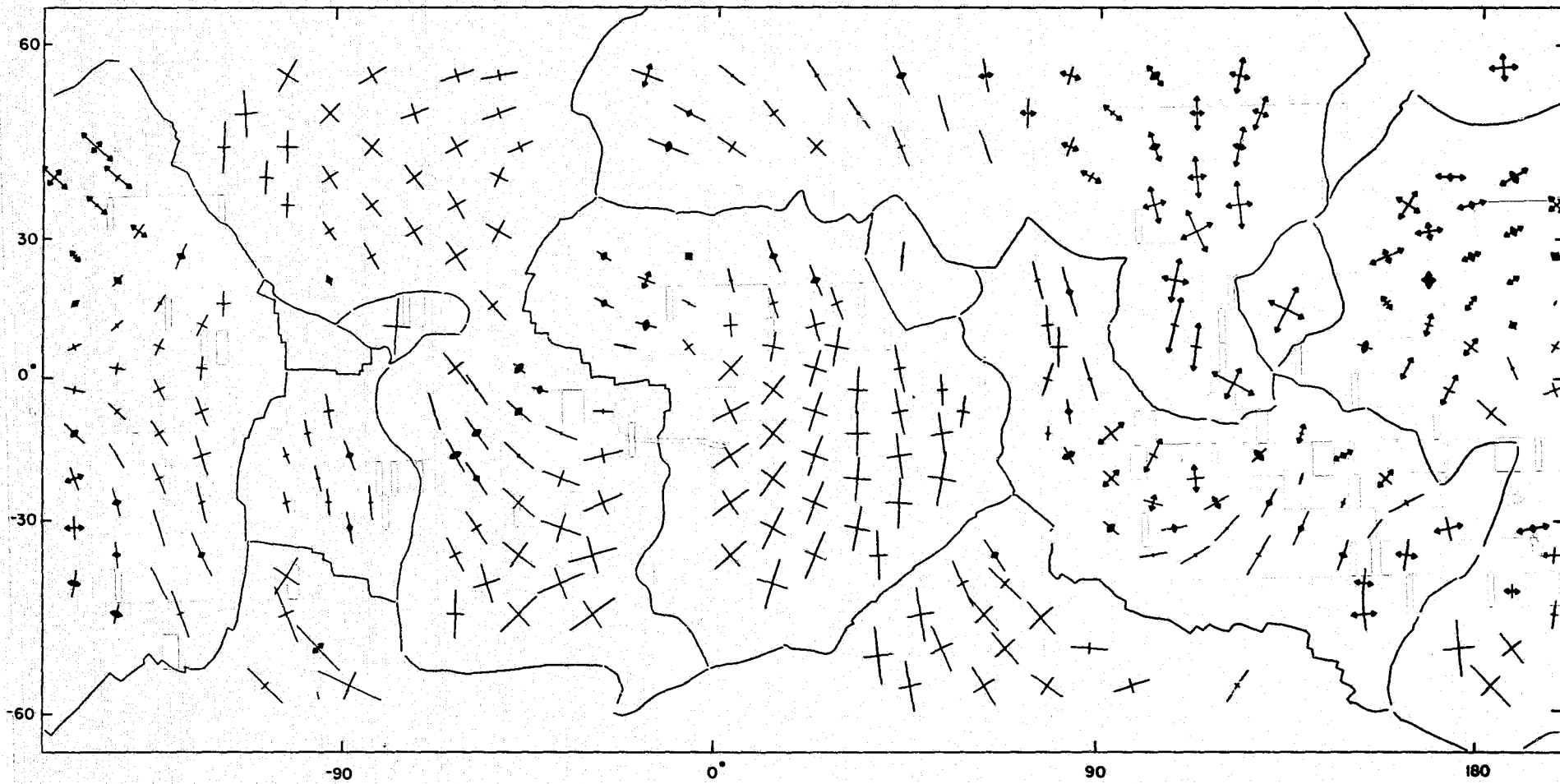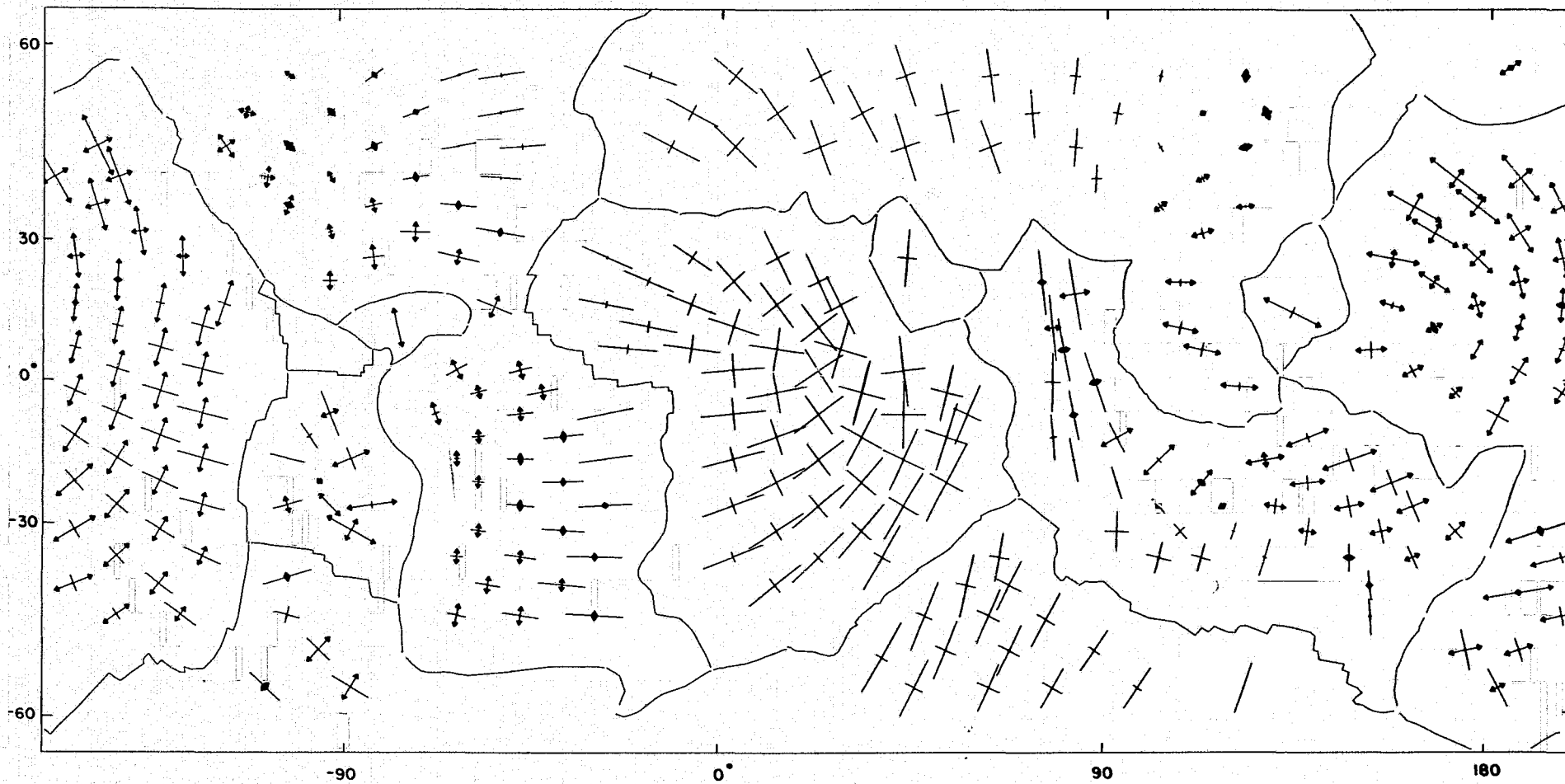INTRAPLATE STRESS FIELD

Figure 1

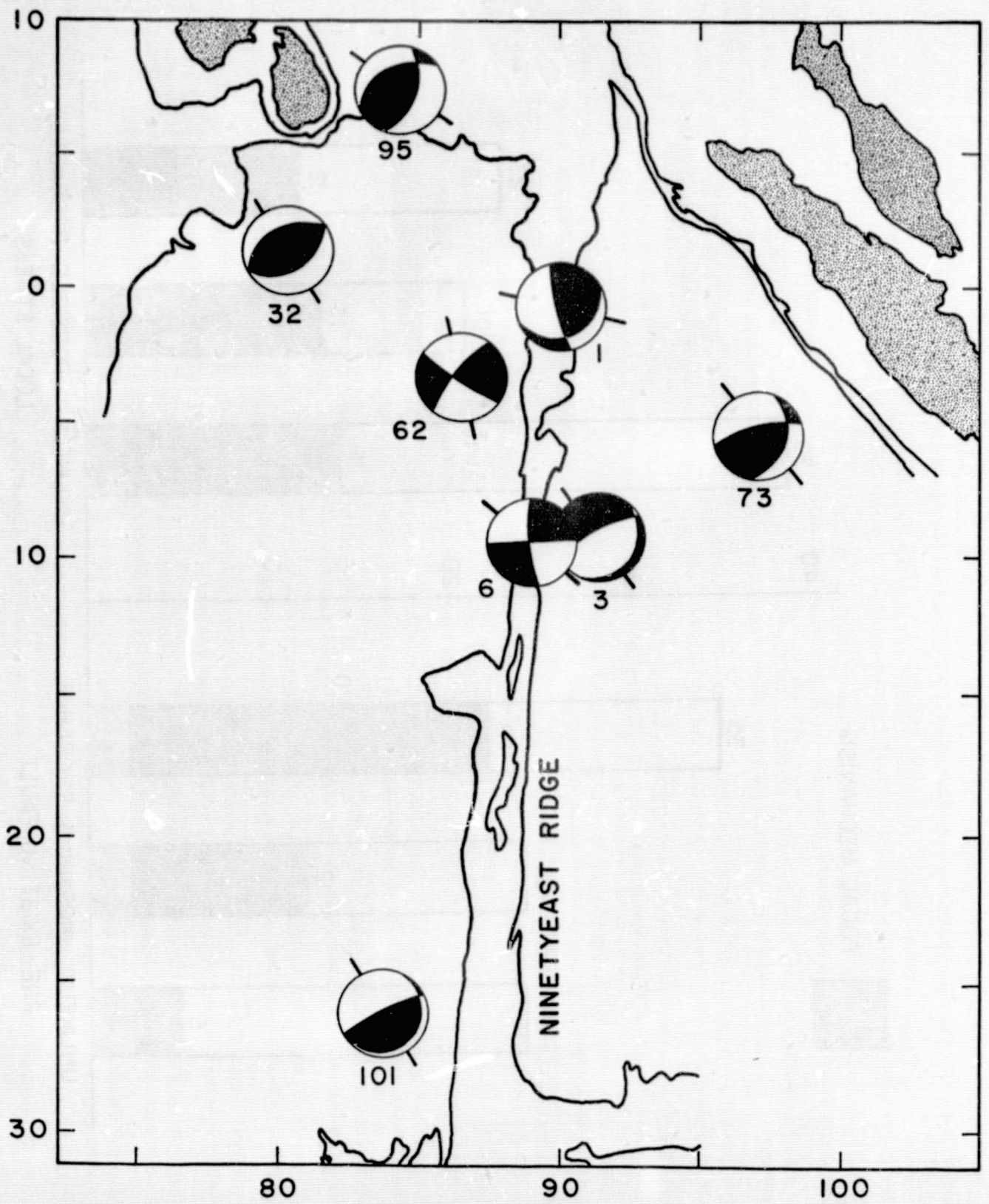MODEL E 31
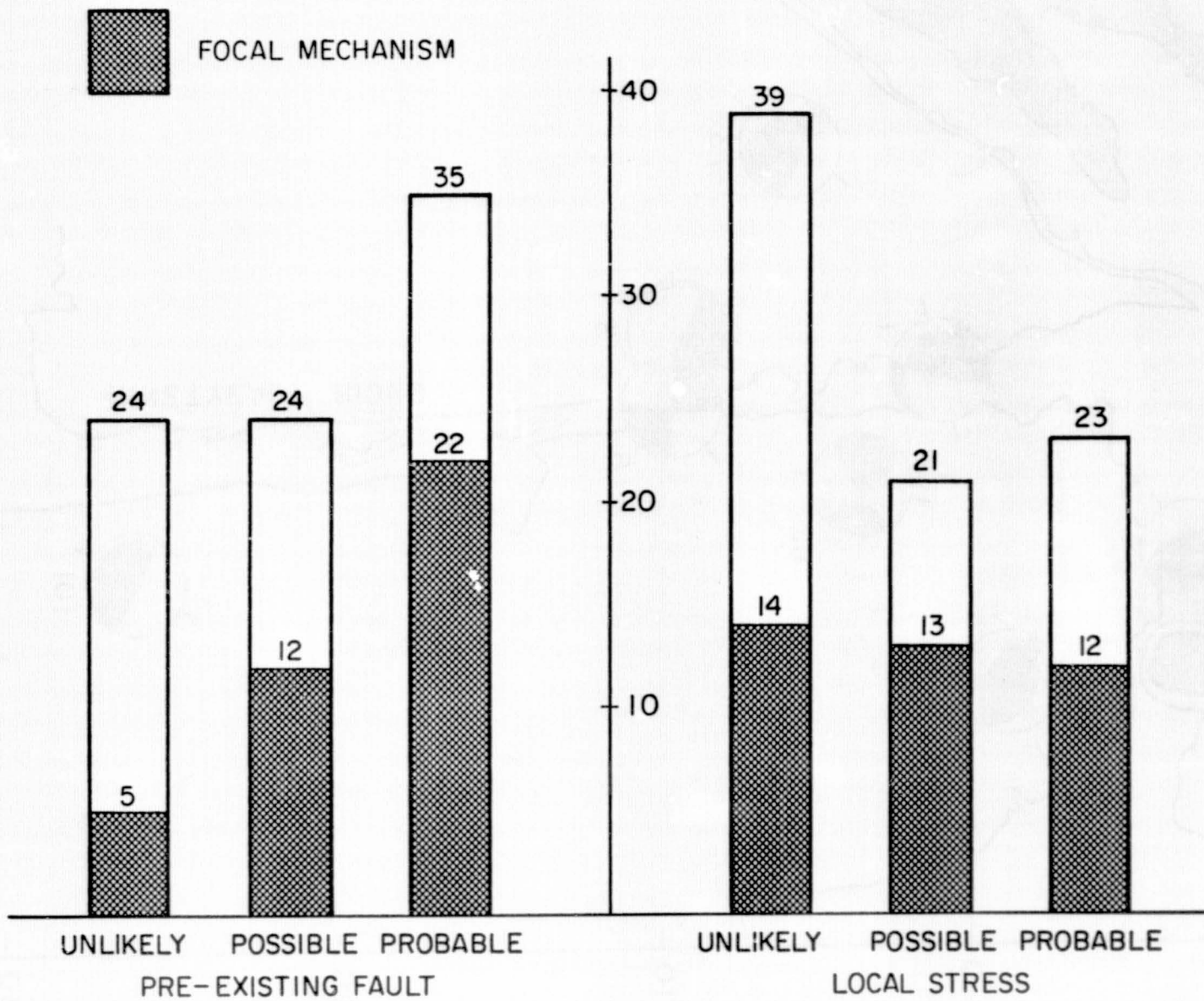
100 bars

Figure 2

MODEL E29

100 bars

Figure 3

Figure 4

Figure 5